NASA TECHNICAL NOTE

NASA TN D-2204

c. 1

NASA TN D-2204

LONGITUDINAL AERODYNAMIC CHARACTERISTICS AND SURFACE PRESSURE MEASUREMENTS FOR A 1/10-SCALE MODEL OF THE RAM B LAUNCH VEHICLE

by Thomas C. Kelly and Robert J. Keynton

Langley Research Center

Langley Station, Hampton, Va.

NATIONAL AERONAUTICS AND SPACE ADMINISTRATION • WASHINGTON, D. C. • APRIL 1964

LONGITUDINAL AERODYNAMIC CHARACTERISTICS AND SURFACE PRESSURE MEASUREMENTS FOR A 1/10-SCALE MODEL OF THE RAM B LAUNCH VEHICLE

By Thomas C. Kelly and Robert J. Keynton

Langley Research Center
Langley Station, Hampton, Va.

NATIONAL AERONAUTICS AND SPACE ADMINISTRATION

For sale by the Office of Technical Services, Department of Commerce,
Washington, D.C. 20230 -- Price $1.00

LONGITUDINAL AERODYNAMIC CHARACTERISTICS AND SURFACE PRESSURE MEASUREMENTS FOR A 1/10-SCALE MODEL OF THE RAM B LAUNCH VEHICLE

By Thomas C. Kelly and Robert J. Keynton
Langley Research Center

SUMMARY

Results have been obtained in the Langley 8-foot transonic pressure tunnel at Mach numbers from about 0.20 to 1.20 for a 1/10-scale model of the RAM B launch vehicle. Force and moment results were obtained over an angle-of-attack range from -6° to 6° and surface pressure distributions were measured over a flare—reverse-flare transition section at angles of attack from -10° to 10° at a Reynolds number per foot on the order of 3.5×10^{6}.

The results indicated that normal-force and pitching-moment characteristics exhibit nonlinear variations over the angle-of-attack range comparable to those noted in NASA Technical Note D-1228 for the related Blue Scout Jr. vehicle, which has fin surfaces similar in arrangement and geometry to those of the present configuration. It is suggested that these nonlinear effects are associated with the downwash field of the forward fins and its effects on the rear fins.

Surface pressure distributions measured over a flare—reverse-flare transition section indicate that the flow over the reverse flare first separates and then reattaches as Mach number is increased from 0.40 to 1.20. This type of flow results in sizable, abrupt pressure variations.

INTRODUCTION

The Langley Research Center of the National Aeronautics and Space Administration is engaged in conducting a series of rocket flight experiments to investigate the interference of ionized flow fields with communications, data transmission, and radar tracking over a wide range of altitudes and velocities. The three-stage launch vehicle (designated RAM B) employed in the flight investigation is a solid-propellant, unguided vehicle. In order to minimize the effects of rocket motor thrust misalinement, the launch vehicle is rotated by means of spin motors which are fired just after the first-stage fins have cleared the launcher. After spin-motor burnout, rotation is maintained by means of aerodynamic control surfaces located at the tips of the first-stage fins. This configuration represents essentially a modified version of the Blue Scout Jr. launch vehicle described in reference 1.

In support of the vehicle development program, an investigation has been conducted in the Langley 8-foot transonic pressure tunnel to determine the static longitudinal aerodynamic characteristics for a 1/10-scale model of the three-stage vehicle at Mach numbers from 0.20 to 1.03 and angles of attack from about -6° to 6°. As a second phase of the experimental investigation, surface pressure distributions were measured over the juncture region of the second and third stages at Mach numbers from 0.40 to 1.20 and angles of attack from -10° to 10° in order to provide information required for the location of vehicle vent openings. Test Reynolds numbers per foot were on the order of 3.5×10^{6}.

SYMBOLS

Aerodynamic force and moment data are referred to the body system of axes, with coefficients based on an area of 0.0522 square foot and a length of 0.258 foot. These values correspond to the body maximum cylindrical cross-sectional area and diameter, respectively. Moments are measured about a point located at 57.1 percent of the model overall length (measured from the theoretical nose-cone apex to the fin trailing edge), or, 6.86 reference diameters forward of the first-stage base.

A — body maximum cylindrical cross-sectional area, sq ft

C_A — axial-force coefficient, $\frac{\text{Axial force}}{qA}$

$C_{A,b}$ — base axial-force coefficient, $\frac{\text{Base axial force}}{qA}$

C_l — rolling-moment coefficient, $\frac{\text{Rolling moment}}{qAd}$

C_m — pitching-moment coefficient, $\frac{\text{Pitching moment}}{qAd}$

C_{m_α} — pitching-moment-curve slope, $\frac{\partial C_m}{\partial \alpha}$, per deg

C_N — normal-force coefficient, $\frac{\text{Normal force}}{qA}$

C_{N_α} — normal-force-curve slope, $\frac{\partial C_N}{\partial \alpha}$, per deg

C_p — pressure coefficient, $\frac{p_l - p}{q}$

d — reference diameter, body maximum cylindrical diameter, in.

l model overall length, measured from theoretical nose-cone apex to fin trailing edge, in.

M Mach number

p free-stream static pressure, lb/sq ft

p_l local static pressure, lb/sq ft

q free-stream dynamic pressure, lb/sq ft

r radius, in.

R Reynolds number per foot

x longitudinal distance, measured from theoretical nose-cone apex, in.

X_{cp} center-of-pressure location in terms of reference diameters forward of model base

α angle of attack of body center line, deg

ϕ orifice-row orientation angle, measured clockwise from vertical as viewed from front, deg

APPARATUS AND PROCEDURE

Model

Details and design dimensions of the 1/10-scale model employed for the present investigation are shown in figure 1(a). The forward set of cruciform-mounted fins had a leading-edge sweepback of 69.1° and utilized single-wedge streamwise airfoil sections with an included angle of 5°. The rear set of fins (first-stage fins), also cruciform-mounted and in line with the forward fins, had a leading-edge sweep of 45.1° and single-wedge streamwise sections with an included angle of 7.8°. All fin leading edges were rounded, with a radius of curvature (measured normal to the leading edge) of 0.025 inch. As may be noted in figure 2, the outer portion (24 percent of the exposed panel span) of each rear fin was deflected (to induce spin). The hinge line for the fin tip control was located at the 68-percent control-root-chord point. For the present investigation, the control surfaces were deflected 6° in a direction to produce positive rolling moment.

Pressure distributions were measured over the region of the flare—reverse-flare transition section (juncture of the second and third stages) by using 24 orifices which were installed in a single, closely spaced, row. Orifice locations used in the tables of results are given in figure 1(b). Model photographs are provided in figure 2.

Procedure

As previously noted, this investigation consisted essentially of two phases. During the initial phase, the longitudinal aerodynamic force and moment characteristics were determined for a 1/10-scale model of the three-stage vehicle through a Mach number range from 0.20 to 1.03 and at angles of attack from -6° to 6°. The effectiveness of the first-stage fins was determined during this portion of the investigation. During the second phase of the investigation, surface pressure distributions were measured over the flare—reverse-flare transition region of the model at Mach numbers from 0.40 to 1.20 and at angles of attack from -10° to 10°. The model was tested with the single orifice row at orientation angles of 0° and 90°.

Reynolds numbers for the investigation are given in figure 3. Differences in Reynolds numbers between the force and pressure-distribution tests below a Mach number of 0.80 result from an attempt to improve the accuracy of the force-test results at Mach numbers of 0.20 and 0.40 by increasing tunnel stagnation pressure.

All tests were conducted with a transition strip located 3.15 inches rearward of the theoretical nose-cone apex. The transition strip was about 0.1 inch wide and was composed of No. 60 carborundum grains set in a plastic adhesive.

Effects of subsonic boundary interference in the slotted test section are considered negligible and no corrections for these effects have been applied. At supersonic speeds, the data are generally affected by boundary-reflected disturbances which occur at Mach numbers from slightly over 1.03 to those at which the disturbances are reflected downstream of the model base. For the force-test phase of the present investigation, the model length and tunnel-power restrictions precluded the attainment of a Mach number at which the model would be free of reflections; therefore, no results are presented for Mach numbers higher than 1.03. Pressure-distribution results are presented for a Mach number of 1.20, however, since the reflections at this Mach number occur well rearward of the model pressure orifices; thus, the reflected disturbances would have no effect on the measured surface pressures.

Axial-force results contained herein have been adjusted to the condition of free-stream static pressure acting at the model base. In addition, angles of attack have been adjusted for tunnel airflow angularity and for deflection of the model and sting support under load.

PRESENTATION OF RESULTS

In order to facilitate presentation of the data, staggered scales have been used in some of the figures and care should be taken in selecting the proper zero axis for each curve. Center-of-pressure results are given in terms of model reference diameters forward of the model base. A list of figures presenting results of this investigation is given below:

Pressure coefficients for the flare—reverse-flare transition section are presented for $\phi = 0^{\circ}$ and $\phi = 90^{\circ}$ in tables I and II, respectively.

DISCUSSION

Force and Moment Characteristics

Results of the force-test phase of the investigation are presented in figures 4 to 7 and are summarized in figure 8. It should be noted here that there is no apparent explanation for the positive normal-force coefficients shown at an angle of attack of 0° for the complete configuration in figure 4(a). This apparent shift should be taken into consideration, however, in obtaining any absolute values of normal-force coefficient for the complete configuration. Examination of the results presented in figures 4 and 6 indicates that, at low angles of attack, the nonlinearities that are evident in the curves for the complete configuration appear only slightly in the results for the configuration with the rear fins (first stage) removed. As noted in reference 1, the nonlinearities are a probable result of the downwash field of the forward fins (which affects the rear fins) and cause a relative reduction in the values of the normal-force-curve slope measured near an angle of attack of 0° for the complete configuration. The increment in normal-force-curve slope resulting from addition of the rear fins is roughly equal to that associated with addition of similar, but slightly smaller, fins to the configuration of reference 1, as would be expected. Center-of-pressure results, given in figures 7 and 8, indicate only small variations resulting from changes in either angle of attack or Mach number. Removal of the rear fins results in a forward shift in center-of-pressure location of about 5 reference diameters, or about 30 percent of the overall model length. Similar center-of-pressure variations may be noted in the results of reference 1.

Axial-force results, given in figures 5 and 8(b), generally show expected variations. A comparison of the present results with those of reference 1 indicates a noticeable increase in the transonic axial-force rise for the present configuration. For example, for the complete configuration, axial-force coefficients at Mach numbers of 0.40 and 1.03 and an angle of attack of 0° amount to 0.45 and 1.26, respectively; whereas, corresponding values from reference 1 are 0.39 and 0.91. Examination of the results of the present investigation and those of reference 1 indicates that the sizable increase in the axial-force rise noted is associated primarily with the transition-flare region. Base axial-force coefficients for the complete configuration of the present investigation are slightly higher than those for the similar configuration of reference 1 at Mach numbers higher than 0.80. This effect is apparently associated with the placement of the rear fins relative to the base. (See fig. 1(a) in ref. 1.)

An indication of the effectiveness of the rear-fin control surfaces in producing rolling moment is given in figure 9. These results show that an increment in rolling-moment coefficient of about 0.20 is realized with the 6° control deflection throughout the Mach number and angle-of-attack ranges.

Surface Pressure Distributions

Surface pressure distributions for the flare—reverse-flare transition section are presented for an angle of attack of 0° for several Mach numbers in figure 10. Examination of these results with particular regard to the flow characteristics over the reverse-flare region shows an interesting variation. At the lowest test Mach numbers, the flow is apparently attached over the reverse-flare surface; however, as Mach number is increased the flow begins to separate just rearward of the flare—reverse-flare corner. The first indication of this onset of separation appears at a Mach number of 0.65 (fig. 10). Further increases in Mach number are accompanied by a rearward spread of the separated region to a condition where the flow is separated over most of the reverse flare at a Mach number of 0.85. Comparison of the curves for Mach numbers of 0.85 and 0.90 indicates a tendency toward flow reattachment on the reverse flare, whereas results for a Mach number of 0.95 are typical of those for the condition where the flow is attached. Further increases in Mach number result in a general increase in pressure coefficients over the reverse flare. Schlieren photographs, presented in figure 11 for Mach numbers from 0.60 to 1.20, indicate a notable change in flow characteristics between Mach numbers of 0.90 and 0.95 which is associated with the flow reattachment.

As noted in reference 2 the variations in local pressure coefficients over the vehicle surface, as well as the abrupt changes in the values of the pressure coefficients with small Mach number changes in flight, may cause the critical local burst or collapse loads across the vehicle outer structure to occur at subsonic or transonic Mach numbers rather than at the higher Mach numbers corresponding to the maximum flight dynamic pressure. The critical loading depends, of course, upon venting arrangements; however, examination of the results of figure 10 indicates that the sudden increase in the value of the negative pressure coefficients over the reverse flare between Mach numbers of 0.90 and 0.95 (which in flight would occur in less than one-half of a second) may, in itself, impose a serious restraint on design of the local structure as well as the vent openings.

Results presented in figure 12 are for an orifice-row orientation angle of 0° and generally indicate slight effects with increasing angle of attack. At Mach numbers of 1.00 and 1.20, however, there are indications of separation originating just rearward of the flare—reverse-flare corner at angles of attack higher than 3°.

Results for an orifice-row orientation angle of 90° for angles of attack from 3° to 10° are presented in figure 13. A comparison of these results with the results given in figure 12 indicates that the most noticeable effects of orifice-row orientation angle are apparent over the region rearward of the reverse flare.

SUMMARY OF RESULTS

An investigation of the static longitudinal aerodynamic characteristics and partial surface pressure distributions for a 1/10-scale model of the RAM B launch vehicle has indicated the following results:

1. Normal-force and pitching-moment characteristics exhibit nonlinear variations over the angle-of-attack range comparable to those noted for the related Blue Scout Jr. vehicle in NASA Technical Note D-1228. It is suggested that these nonlinear effects are associated with the downwash field of the forward fins and its effects on the rear fins.

2. Surface pressure distributions measured over a flare—reverse-flare transition section indicate that the flow over the reverse flare first separates and then reattaches as Mach number is increased from 0.40 to 1.20. This type of flow results in sizable, abrupt pressure variations.

Langley Research Center,
National Aeronautics and Space Administration,
Langley Station, Hampton, Va., December 24, 1963.

REFERENCES

1. Kelly, Thomas C., and Keynton, Robert J.: Investigation of the Static Longitudinal Aerodynamic Characteristics of a 1/10-Scale Model of the Blue Scout Jr. at Mach Numbers From 0.40 to 1.03. NASA TN D-1228, 1962.

2. Kelly, Thomas C.: Aerodynamic Loading Characteristics at Mach Numbers From 0.80 to 1.20 of a 1/10-Scale Three-Stage Scout Model. NASA TN D-945, 1961.

TABLE I.- SURFACE PRESSURE COEFFICIENTS FOR FLARE—REVERSE-FLARE

TRANSITION SECTION, $\phi = 0^{\circ}$

(a) M = 0.40 to 0.95; $\alpha = 0^{\circ}$

x/l	C_p for -						
	M = 0.40	M = 0.65	M = 0.70	M = 0.75	M = 0.85	M = 0.90	M = 0.95
0.259	0.262	0.261	0.301	0.315	0.341	0.366	0.401
.263	.308	.305	.344	.357	.380	.406	.440
.278	.095	.084	.129	.145	.181	.212	.262
.296	-.066	-.082	-.032	-.012	.034	.075	.131
.312	-.619	-.553	-.470	-.418	-.293	-.216	-.134
.313	-1.338	-1.060	-.942	-.877	-.764	-.735	-.651
.315	-.787	-.790	-.674	-.612	-.550	-.645	-1.065
.317	-.421	-.738	-.648	-.601	-.544	-.616	-1.036
.321	-.228	-.602	-.576	-.583	-.553	-.601	-.994
.325	-.118	-.424	-.450	-.527	-.563	-.589	-.954
.329	-.040	-.283	-.318	-.436	-.559	-.577	-.915
.332	.017	-.194	-.222	-.347	-.536	-.560	-.892
.335	.084	-.115	-.133	-.246	-.490	-.531	-.646
.338	.107	-.066	-.073	-.175	-.446	-.503	-.455
.342	.065	-.024	-.012	-.081	-.344	-.434	-.388
.347	.049	-.007	.021	-.022	-.245	-.358	-.335
.352	.033	-.005	.003	.013	-.161	-.276	-.290
.356	.023	-.006	.038	.037	-.086	-.198	-.231
.361	.010	-.016	.028	.034	-.046	-.144	-.176
.375	.005	-.026	.020	.033	.033	-.013	-.020
.395	.009	-.032	.012	.023	.047	.046	.048
.414	.013	-.035	.008	.016	.037	.048	.062
.434	.034	-.012	.031	.036	.048	.059	.076
.453	.039	-.009	.029	.037	.043	.051	.078

TABLE I.- SURFACE PRESSURE COEFFICIENTS FOR FLARE—REVERSE-FLARE

TRANSITION SECTION, $\phi = 0^{\circ}$ - Continued

(b) $M = 0.60$; $\alpha = -10^{\circ}$ to 10°

x/l	C_p for -						
	$\alpha = -10^{\circ}$	$\alpha = -6^{\circ}$	$\alpha = -3^{\circ}$	$\alpha = 0^{\circ}$	$\alpha = 3^{\circ}$	$\alpha = 6^{\circ}$	$\alpha = 10^{\circ}$
0.259	0.399	0.355	0.330	0.286	0.243	0.220	0.236
.263	.488	.431	.390	.331	.273	.256	.332
.278	.242	.185	.154	.118	.083	.068	.052
.296	.083	.023	-.011	-.045	-.079	-.094	-.101
.312	-.492	-.526	-.532	-.535	-.516	-.499	-.539
.313	-1.383	-1.281	-1.196	-1.092	-.955	-.920	-1.151
.315	-1.063	-.986	-.916	-.826	-.725	-.677	-.825
.317	-.683	-.754	-.714	-.661	-.582	-.559	-.696
.321	-.318	-.417	-.417	-.406	-.376	-.372	-.416
.325	-.134	-.196	-.217	-.228	-.232	-.230	-.200
.329	-.028	-.069	-.093	-.122	-.140	-.139	-.087
.332	.048	.011	-.014	-.053	-.083	-.086	-.018
.335	.152	.099	.058	.010	-.032	-.031	.065
.338	.191	.140	.097	.046	-.004	-.002	.110
.342	.119	.097	.085	.049	.015	.015	.070
.347	.096	.077	.070	.050	.022	.025	.057
.352	.068	.051	.051	.038	.020	.025	.040
.356	.060	.040	.040	.032	.019	.025	.035
.361	.047	.026	.027	.020	.013	.020	.023
.375	.042	.021	.019	.013	.006	.015	.019
.395	.047	.025	.019	.013	.004	.011	.015
.414	.052	.026	.019	.011	.003	.006	.004
.434	.089	.057	.048	.033	.018	.019	.024
.453	.099	.067	.053	.037	.019	.014	.003

TABLE I.- SURFACE PRESSURE COEFFICIENTS FOR FLARE—REVERSE-FLARE

TRANSITION SECTION, $\phi = 0^{\circ}$ - Continued

(c) M = 0.80; $\alpha = -10^{\circ}$ to 10°

x/l	C_p for -						
	$\alpha = -10^{\circ}$	$\alpha = -6^{\circ}$	$\alpha = -3^{\circ}$	$\alpha = 0^{\circ}$	$\alpha = 3^{\circ}$	$\alpha = 6^{\circ}$	$\alpha = 10^{\circ}$
0.259	0.445	0.405	0.370	0.324	0.281	0.255	0.267
.263	.542	.482	.433	.365	.310	.297	.369
.278	.296	.237	.198	.159	.122	.097	.078
.296	.157	.093	.052	.006	-.035	-.064	-.079
.312	-.228	-.279	-.314	-.363	-.410	-.419	-.393
.313	-.877	-.862	-.846	-.819	-.783	-.781	-.802
.315	-.697	-.628	-.595	-.574	-.559	-.541	-.528
.317	-.686	-.624	-.590	-.567	-.554	-.536	-.530
.321	-.692	-.633	-.599	-.571	-.549	-.534	-.546
.325	-.680	-.639	-.604	-.566	-.523	-.514	-.548
.329	-.606	-.605	-.577	-.527	-.469	-.455	-.507
.332	-.495	-.535	-.517	-.468	-.403	-.387	-.438
.335	-.330	-.423	-.425	-.387	-.324	-.309	-.348
.338	-.194	-.325	-.347	-.321	-.268	-.253	-.278
.342	.027	-.142	-.201	-.206	-.181	-.168	-.163
.347	.132	-.011	-.089	-.118	-.112	-.105	-.079
.352	.148	.060	-.010	-.054	-.063	-.059	-.026
.356	.130	.090	.040	-.004	-.024	-.024	.009
.361	.096	.080	.051	.016	-.006	-.005	.019
.375	.059	.051	.050	.040	.027	.028	.036
.395	.050	.035	.035	.033	.029	.032	.033
.414	.050	.029	.024	.021	.019	.021	.020
.434	.086	.059	.046	.038	.029	.027	.028
.453	.098	.068	.050	.036	.024	.014	.000

TABLE I.- SURFACE PRESSURE COEFFICIENTS FOR FLARE—REVERSE-FLARE TRANSITION SECTION, $\phi = 0^{\circ}$ - Continued

(d) $M = 1.00$; $\alpha = -10^{\circ}$ to 10°

x/l	C_p for -						
	$\alpha = -10^{\circ}$	$\alpha = -6^{\circ}$	$\alpha = -3^{\circ}$	$\alpha = 0^{\circ}$	$\alpha = 3^{\circ}$	$\alpha = 6^{\circ}$	$\alpha = 10^{\circ}$
0.259	0.589	0.564	0.489	0.430	0.388	0.342	0.401
.263	.682	.636	.540	.460	.412	.382	.501
.278	.464	.426	.358	.324	.288	.254	.253
.296	.354	.311	.240	.198	.158	.119	.111
.312	.093	.064	-.004	-.060	-.124	-.144	-.106
.313	-.445	-.459	-.509	-.551	-.596	-.602	-.563
.315	-.893	-.892	-.923	-.941	-.966	-.984	-.975
.317	-.870	-.875	-.905	-.913	-.926	-.966	-.974
.321	-.804	-.826	-.863	-.872	-.861	-.920	-.959
.325	-.742	-.775	-.820	-.834	-.812	-.866	-.943
.329	-.686	-.728	-.778	-.797	-.772	-.792	-.920
.332	-.653	-.703	-.756	-.775	-.753	-.742	-.896
.335	-.394	-.483	-.548	-.541	-.481	-.478	-.616
.338	-.180	-.259	-.335	-.362	-.350	-.356	-.447
.342	-.114	-.198	-.278	-.304	-.303	-.304	-.315
.347	-.085	-.160	-.236	-.260	-.270	-.275	-.217
.352	-.086	-.146	-.214	-.230	-.238	-.242	-.175
.356	-.082	-.130	-.189	-.199	-.203	-.199	-.139
.361	-.094	-.132	-.183	-.185	-.181	-.174	-.122
.375	-.091	-.108	-.134	-.124	-.111	-.105	-.074
.395	-.091	-.073	-.091	-.087	-.078	-.077	-.059
.414	-.065	-.047	-.073	-.071	-.061	-.063	-.047
.434	-.005	-.001	-.035	-.038	-.030	-.025	-.007
.453	.082	.059	.014	.007	.008	-.002	.017

TABLE I.- SURFACE PRESSURE COEFFICIENTS FOR FLARE—REVERSE-FLARE TRANSITION SECTION, $\phi = 0^\circ$ - Concluded

(e) $M = 1.20$; $\alpha = -10^\circ$ to 10°

x/l	C_p for -						
	$\alpha = -10^\circ$	$\alpha = -6^\circ$	$\alpha = -3^\circ$	$\alpha = 0^\circ$	$\alpha = 3^\circ$	$\alpha = 6^\circ$	$\alpha = 10^\circ$
0.259	0.479	0.442	0.406	0.356	0.300	0.260	0.351
.263	.594	.523	.463	.388	.317	.297	.528
.278	.535	.477	.435	.385	.330	.308	.319
.296	.465	.401	.354	.311	.268	.250	.242
.312	.296	.247	.200	.140	.059	.072	.103
.313	-.153	-.186	-.220	-.260	-.315	-.299	-.263
.315	-.541	-.554	-.569	-.578	-.595	-.629	-.622
.317	-.529	-.544	-.556	-.556	-.559	-.634	-.629
.321	-.492	-.517	-.532	-.531	-.524	-.606	-.631
.325	-.454	-.485	-.506	-.508	-.495	-.539	-.624
.329	-.418	-.457	-.480	-.483	-.466	-.444	-.594
.332	-.402	-.443	-.470	-.472	-.453	-.403	-.544
.335	-.281	-.331	-.357	-.333	-.253	-.225	-.317
.338	-.042	-.106	-.145	-.158	-.147	-.138	-.208
.342	-.023	-.087	-.127	-.132	-.127	-.105	-.116
.347	-.002	-.064	-.103	-.110	-.110	-.107	-.075
.352	-.002	-.060	-.097	-.100	-.103	-.109	-.089
.356	.000	-.054	-.088	-.088	-.092	-.098	-.096
.361	-.004	-.056	-.088	-.086	-.088	-.093	-.095
.375	-.001	-.048	-.066	-.062	-.060	-.054	-.042
.395	-.001	-.039	-.040	-.042	-.038	-.032	-.020
.414	-.011	-.034	-.033	-.027	-.028	-.022	-.016
.434	.008	.008	-.005	-.006	-.009	.002	.011
.453	.003	-.004	-.007	-.004	-.002	.004	-.001

TABLE II.- SURFACE PRESSURE COEFFICIENTS FOR FLARE—REVERSE-FLARE TRANSITION SECTION, $\phi = 90^\circ$

(a) M = 0.60

x/l	C_p for -		
	$\alpha = 3^\circ$	$\alpha = 6^\circ$	$\alpha = 10^\circ$
0.259	0.282	0.266	0.193
.263	.326	.313	.241
.278	.104	.078	.004
.296	-.052	-.070	-.128
.312	-.540	-.553	-.596
.313	-1.072	-1.071	-1.070
.315	-.791	-.775	-.782
.317	-.674	-.678	-.695
.321	-.449	-.484	-.531
.325	-.264	-.304	-.359
.329	-.143	-.172	-.221
.332	-.069	-.090	-.135
.335	-.007	-.021	-.056
.338	.033	.019	-.014
.342	.040	.026	-.022
.347	.042	.025	-.030
.352	.032	.009	-.057
.356	.024	.000	-.069
.361	.011	-.015	-.083
.375	.003	-.023	-.093
.395	.002	-.022	-.095
.414	.001	-.025	-.091
.434	.027	.004	-.059
.453	.030	.001	-.066

(b) M = 0.80

x/l	C_p for -		
	$\alpha = 3^\circ$	$\alpha = 6^\circ$	$\alpha = 10^\circ$
0.259	0.324	0.312	0.242
.263	.365	.356	.286
.278	.150	.124	.048
.296	.003	-.014	-.079
.312	-.360	-.363	-.413
.313	-.772	-.726	-.690
.315	-.548	-.519	-.513
.317	-.545	-.514	-.503
.321	-.550	-.520	-.507
.325	-.546	-.520	-.505
.329	-.526	-.509	-.495
.332	-.491	-.486	-.479
.335	-.430	-.442	-.447
.338	-.380	-.409	-.427
.342	-.271	-.323	-.368
.347	-.172	-.225	-.286
.352	-.088	-.131	-.193
.356	-.027	-.059	-.113
.361	.002	-.023	-.076
.375	.033	.013	-.050
.395	.022	.000	-.074
.414	.011	-.010	-.082
.434	.030	.011	-.050
.453	.029	.011	-.037

TABLE II.- SURFACE PRESSURE COEFFICIENTS FOR FLARE—REVERSE-FLARE

TRANSITION SECTION, $\phi = 90^{\circ}$ - Concluded

(c) M = 1.00

x/l	C_p for -		
	$\alpha = 3^{\circ}$	$\alpha = 6^{\circ}$	$\alpha = 10^{\circ}$
0.259	0.440	0.435	0.371
.263	.473	.475	.410
.278	.321	.288	.211
.296	.203	.180	.113
.312	-.046	-.057	-.114
.313	-.533	-.536	-.572
.315	-.936	-.946	-.974
.317	-.918	-.935	-.964
.321	-.883	-.901	-.931
.325	-.847	-.867	-.899
.329	-.809	-.831	-.866
.332	-.787	-.803	-.835
.335	-.585	-.625	-.636
.338	-.373	-.387	-.420
.342	-.319	-.347	-.379
.347	-.265	-.298	-.343
.352	-.229	-.265	-.329
.356	-.195	-.229	-.317
.361	-.180	-.210	-.308
.375	-.124	-.155	-.258
.395	-.090	-.123	-.206
.414	-.075	-.103	-.178
.434	-.038	-.058	-.119
.453	.014	.021	.022

(d) M = 1.20

x/l	C_p for -		
	$\alpha = 3^{\circ}$	$\alpha = 6^{\circ}$	$\alpha = 10^{\circ}$
0.259	0.358	0.346	0.278
.263	.392	.379	.303
.278	.381	.349	.271
.296	.312	.289	.225
.312	.150	.145	.087
.313	-.249	-.249	-.285
.315	-.580	-.590	-.618
.317	-.565	-.581	-.614
.321	-.545	-.565	-.596
.325	-.523	-.545	-.578
.329	-.500	-.523	-.559
.332	-.487	-.507	-.544
.335	-.376	-.411	-.449
.338	-.174	-.194	-.243
.342	-.158	-.187	-.235
.347	-.131	-.164	-.216
.352	-.118	-.156	-.212
.356	-.104	-.147	-.215
.361	-.096	-.138	-.217
.375	-.064	-.098	-.197
.395	-.044	-.076	-.168
.414	-.038	-.071	-.153
.434	-.006	-.037	-.113
.453	-.016	-.053	-.102

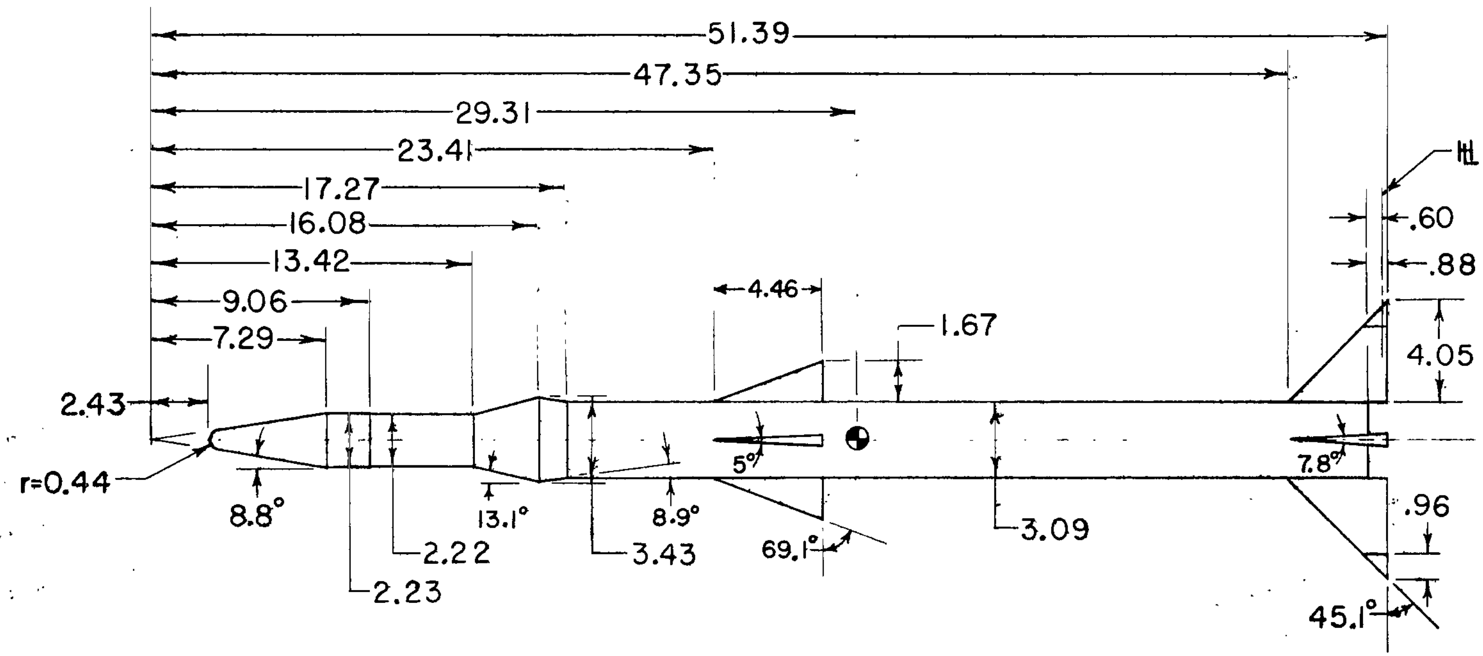

(a) Complete force-test configuration.

Figure 1.- Model details. All dimensions are in inches unless otherwise noted.

x, in.	x/l	x, in.	x/l
13.28	0.259	17.20	0.335
13.47	.263	17.35	.338
14.27	.278	17.57	.342
15.17	.296	17.79	.347
16.00	.312	18.04	.352
16.06	.313	18.28	.356
16.16	.315	18.51	.361
16.27	.317	19.24	.375
16.47	.321	20.25	.395
16.67	.325	21.25	.414
16.87	.329	22.26	.434
17.02	.332	23.26	.453

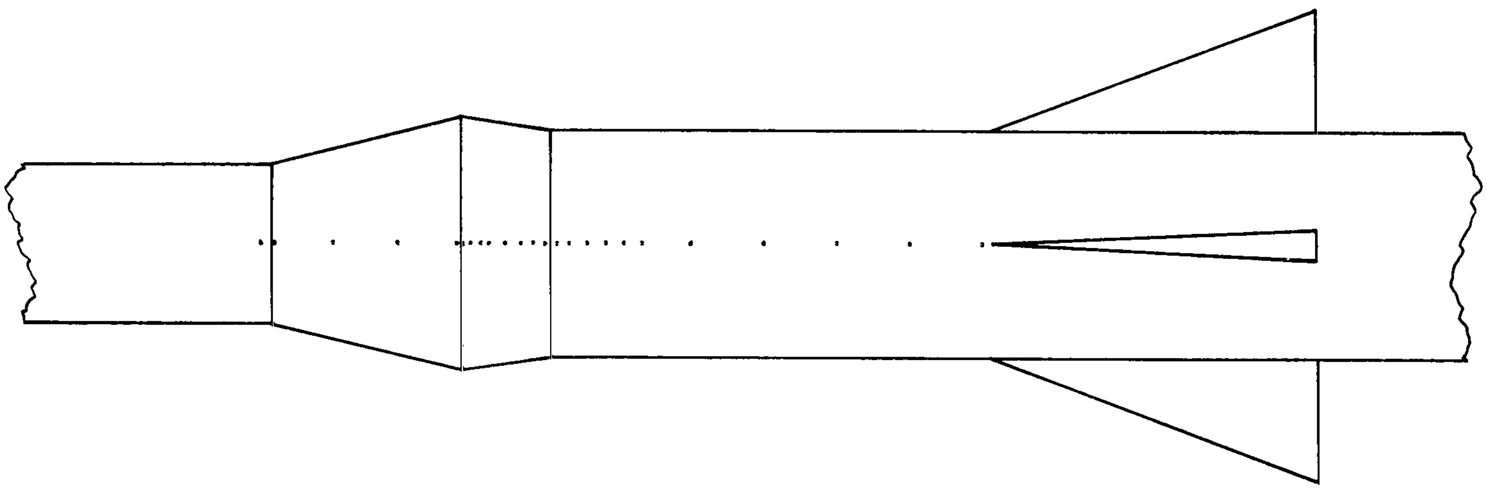

(b) Orifice locations on flare—reverse-flare section.

Figure 1.- Concluded.

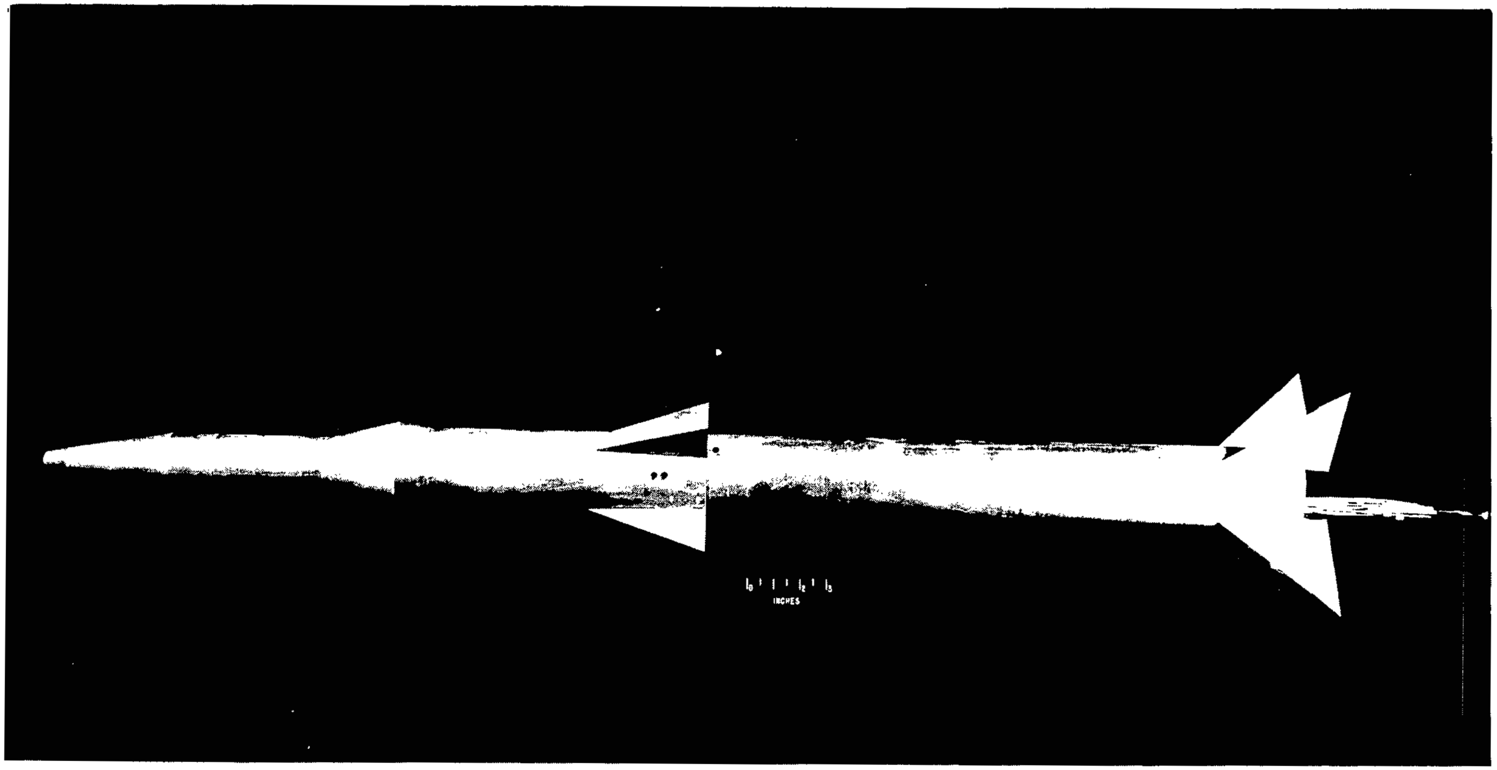

(a) Complete basic configuration. L-63-6933

Figure 2.- Model photographs.

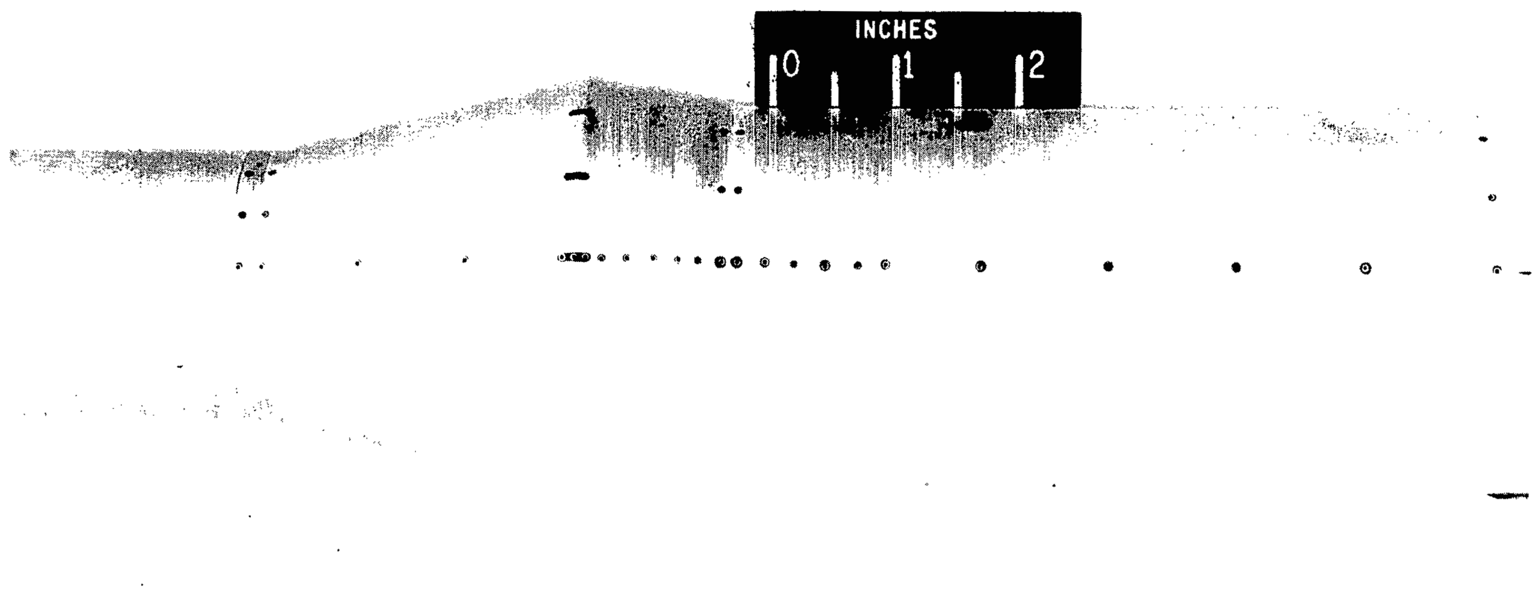

(b) Flare—reverse-flare details.

L-63-6334

Figure 2.- Continued.

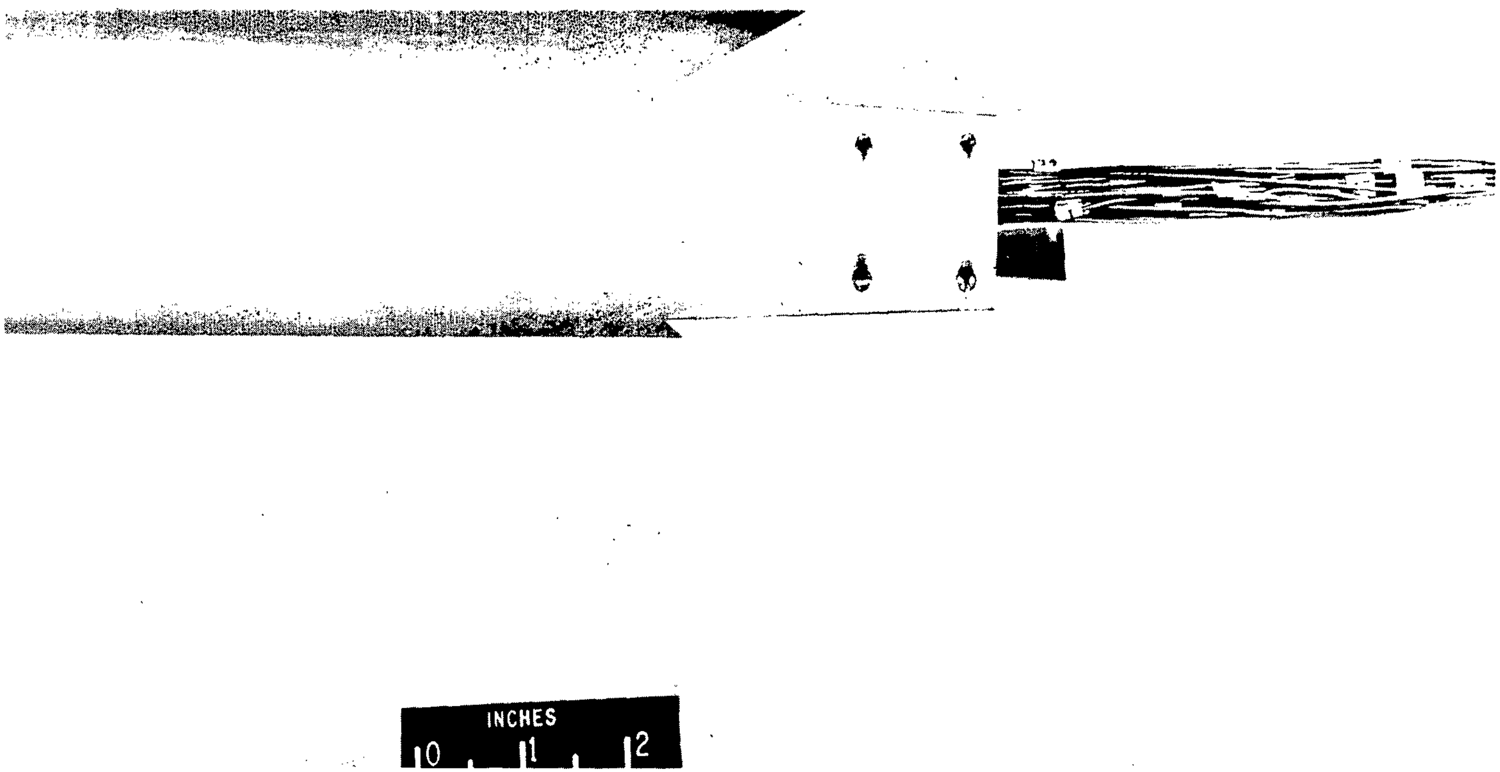

(c) Base-fin and tip-control details. L-63-6333

Figure 2.- Concluded.

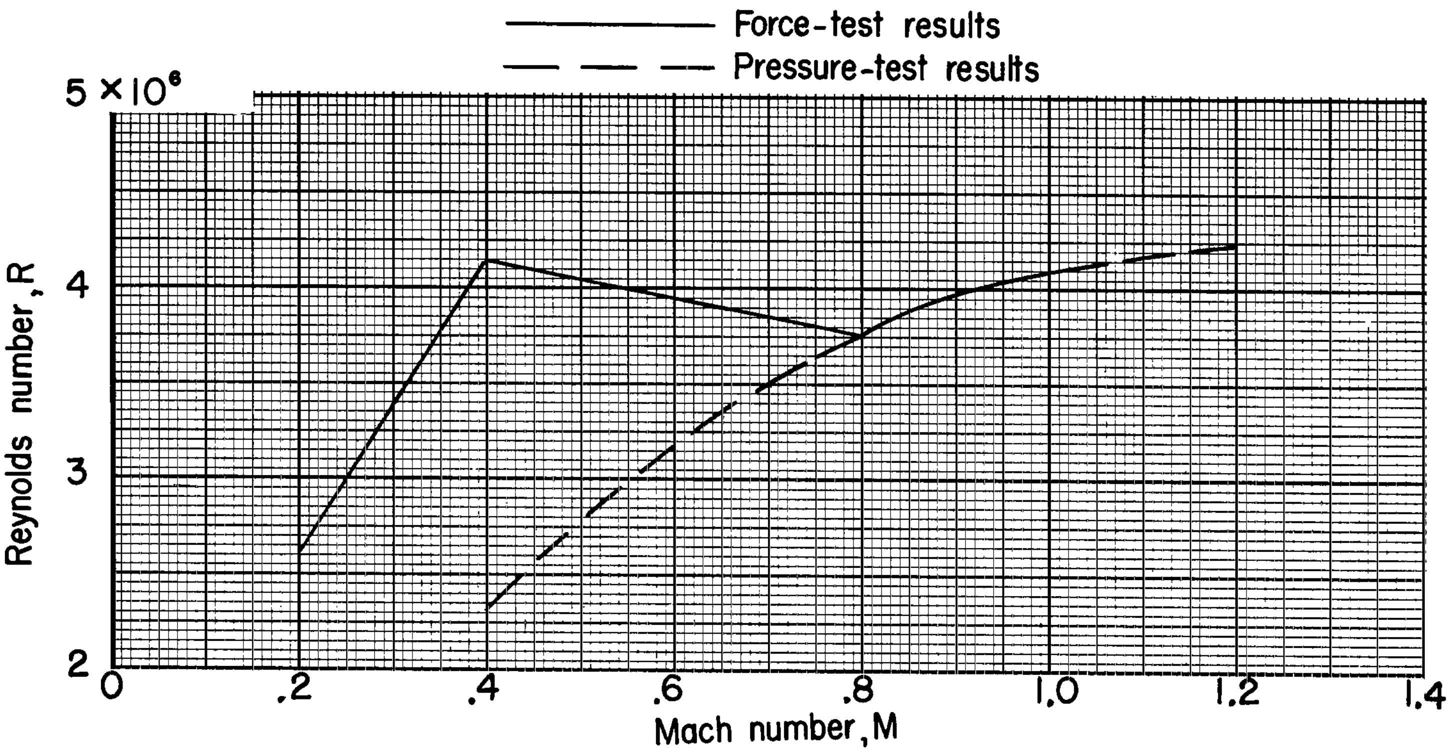

Figure 3.- Variation of average test Reynolds number per foot with Mach number.

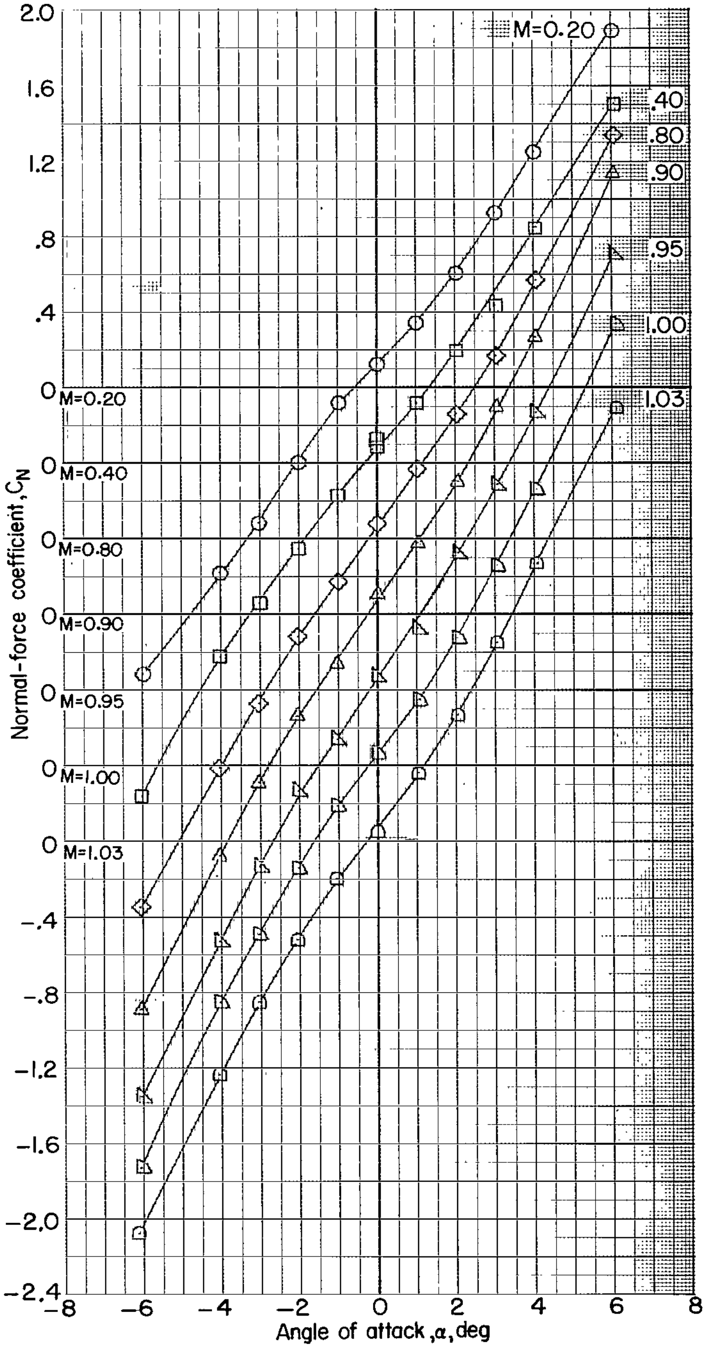

(a) Complete configuration.

Figure 4.- Variation of normal-force coefficient with angle of attack.

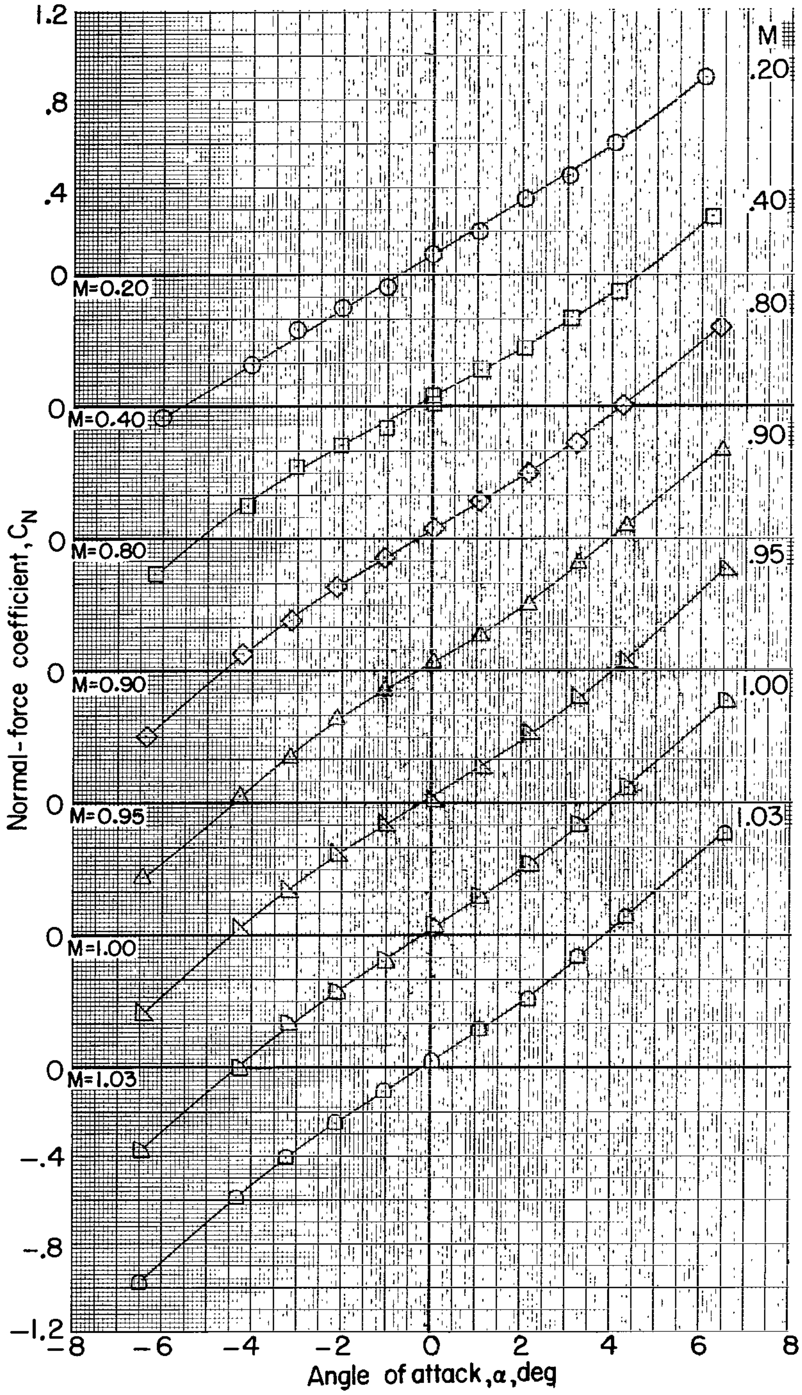

(b) First-stage fins off.

Figure 4.- Concluded.

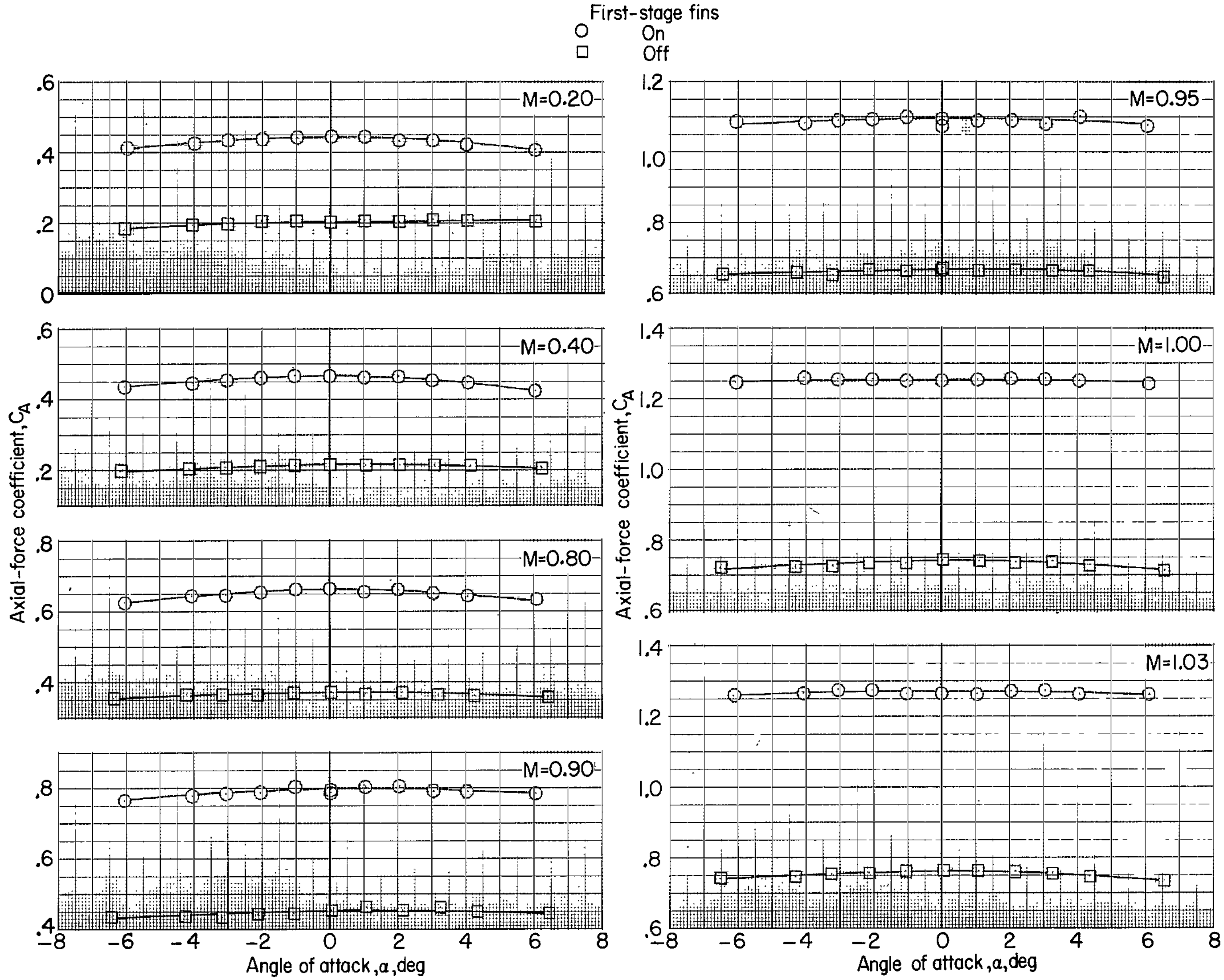

(a) Axial-force coefficients.

Figure 5.- Variation of axial-force coefficient with angle of attack.

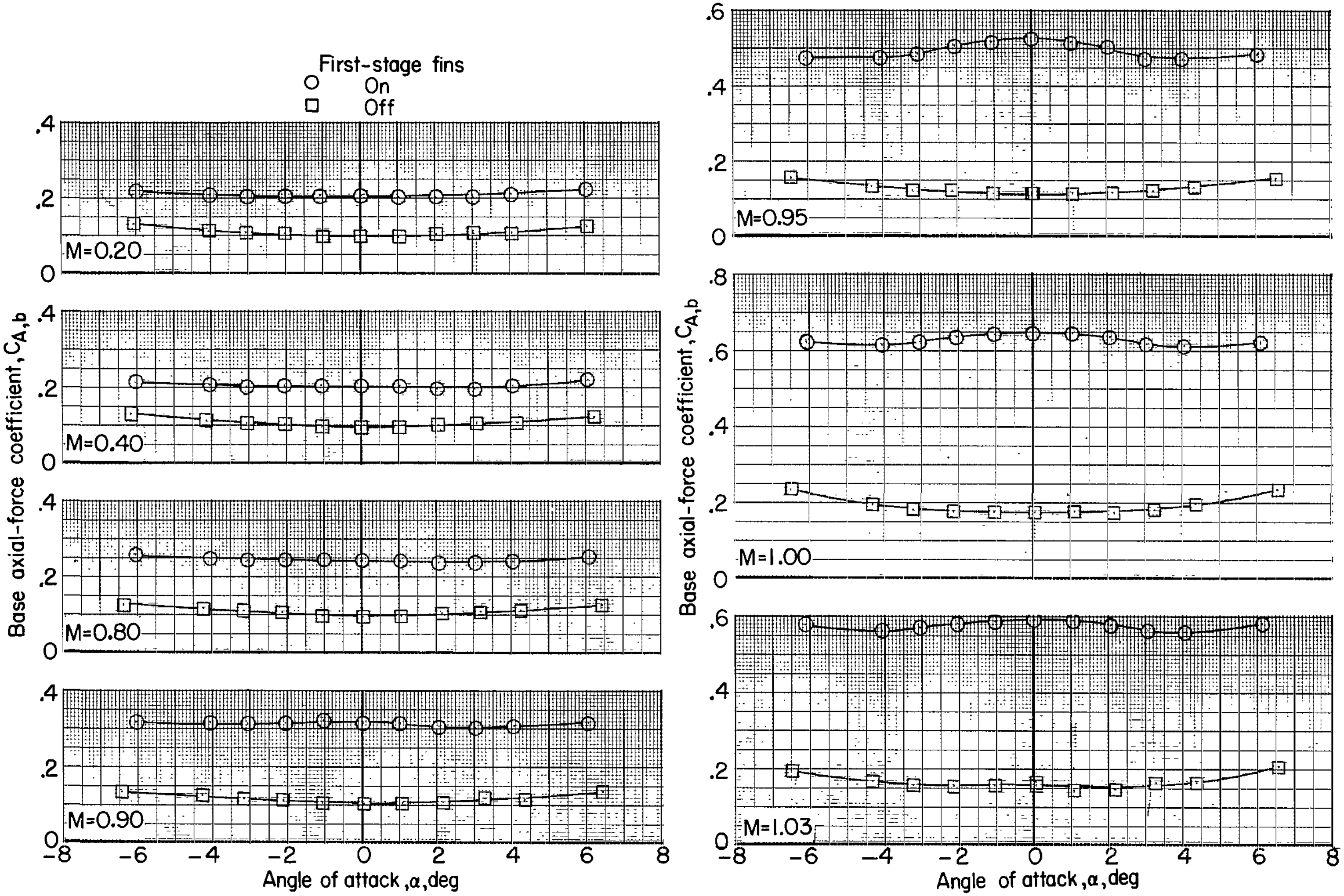

(b) Base axial-force coefficients.

Figure 5.- Concluded.

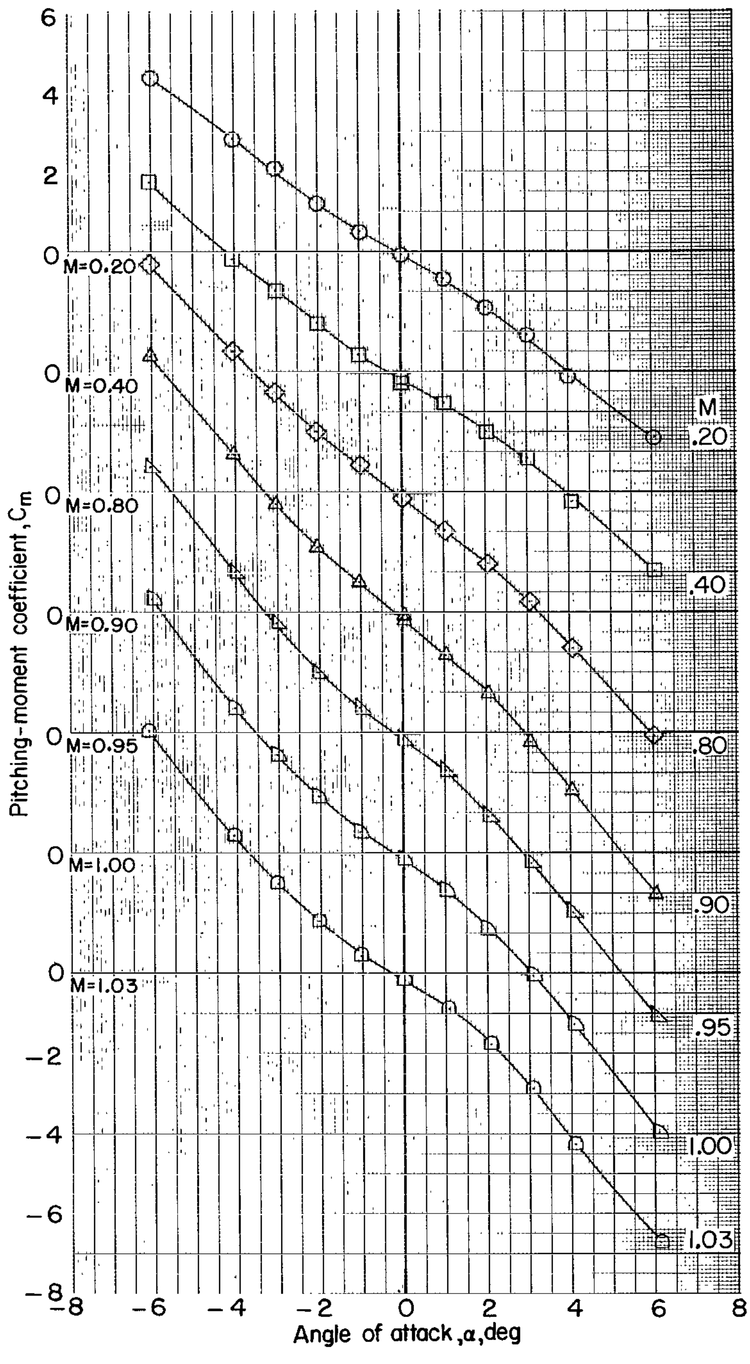

(a) Complete configuration.

Figure 6.- Variation of pitching-moment coefficient with angle of attack.

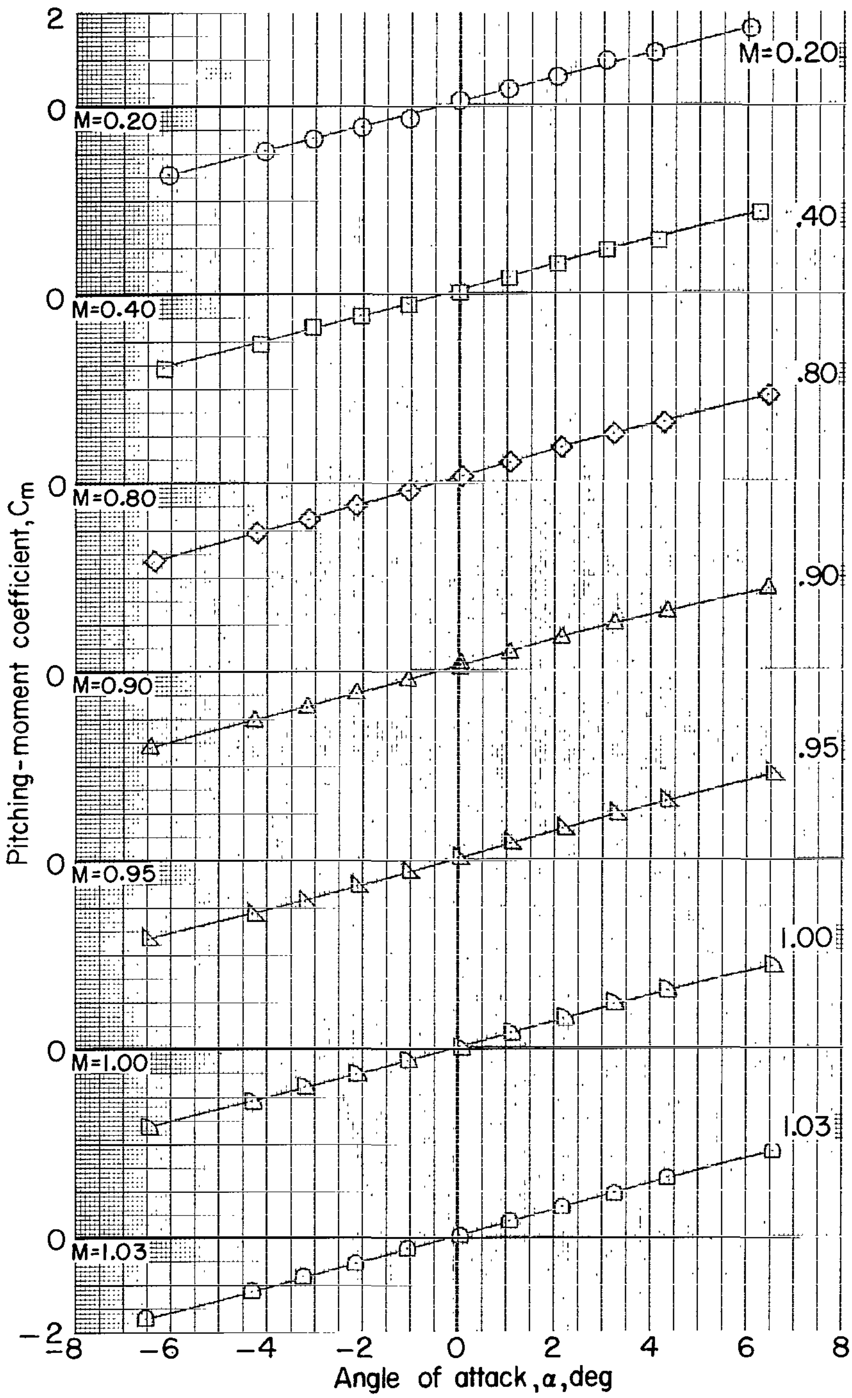

(b) First-stage fins off.

Figure 6.- Concluded.

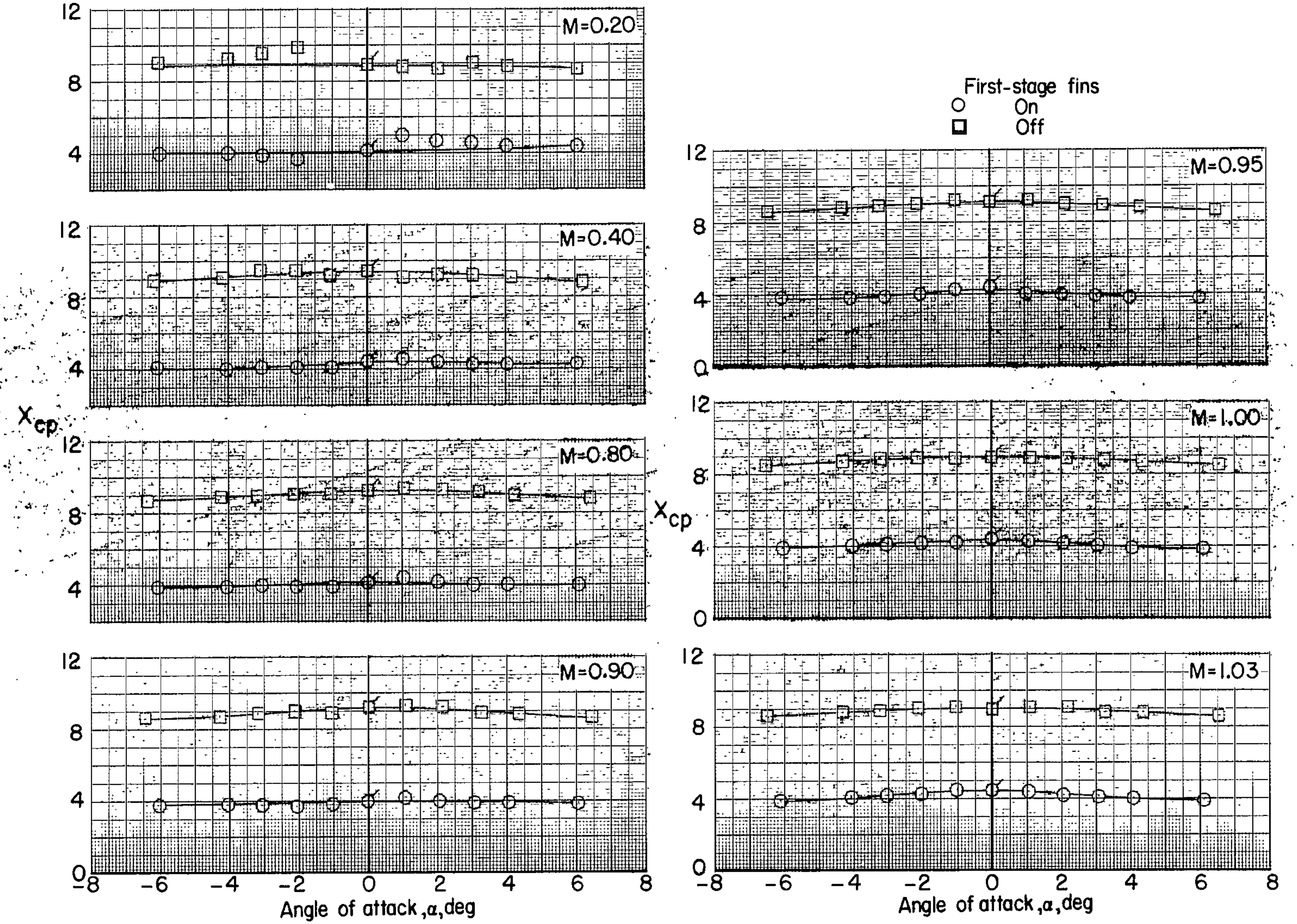

Figure 7.- Variation of center-of-pressure location with angle of attack. (Flagged symbols indicate points computed by using C_{m_α} and C_{N_α}.)

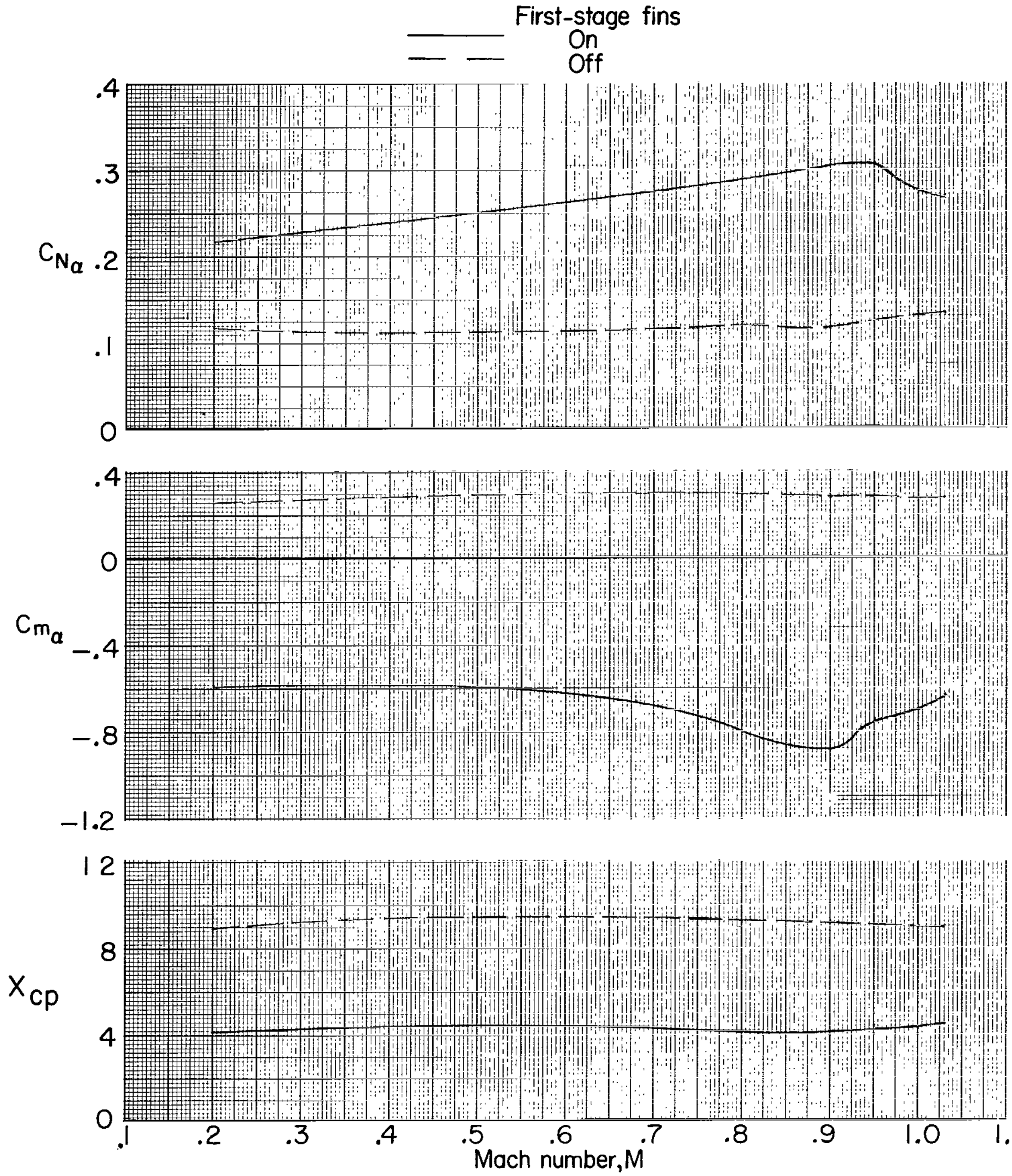

(a) C_{N_α}, C_{m_α}, and X_{cp} plotted against Mach number.

Figure 8.- Summary of aerodynamic characteristics in pitch. $\alpha = 0^\circ$.

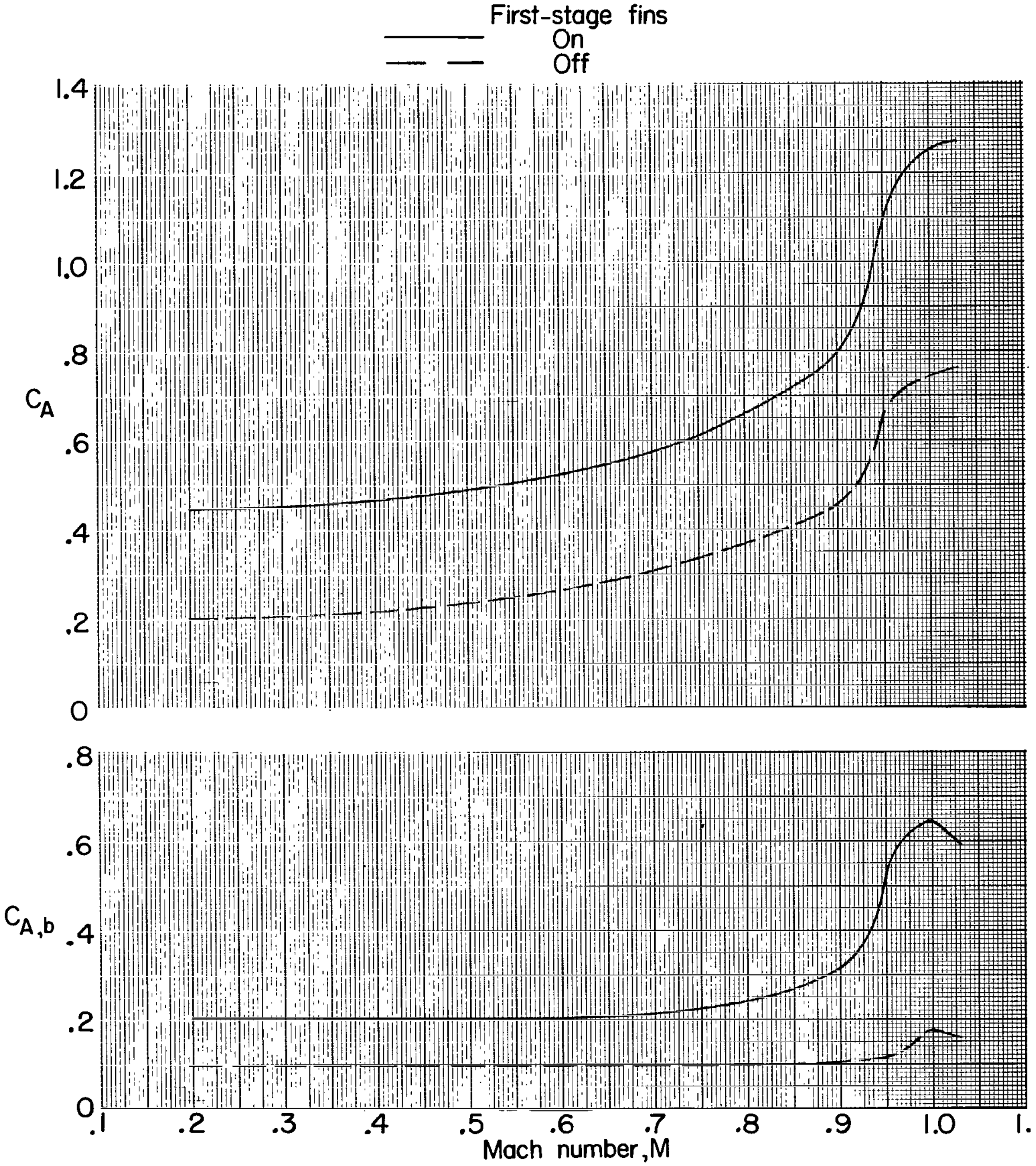

(b) C_A and $C_{A,b}$ plotted against Mach number.

Figure 8.- Concluded.

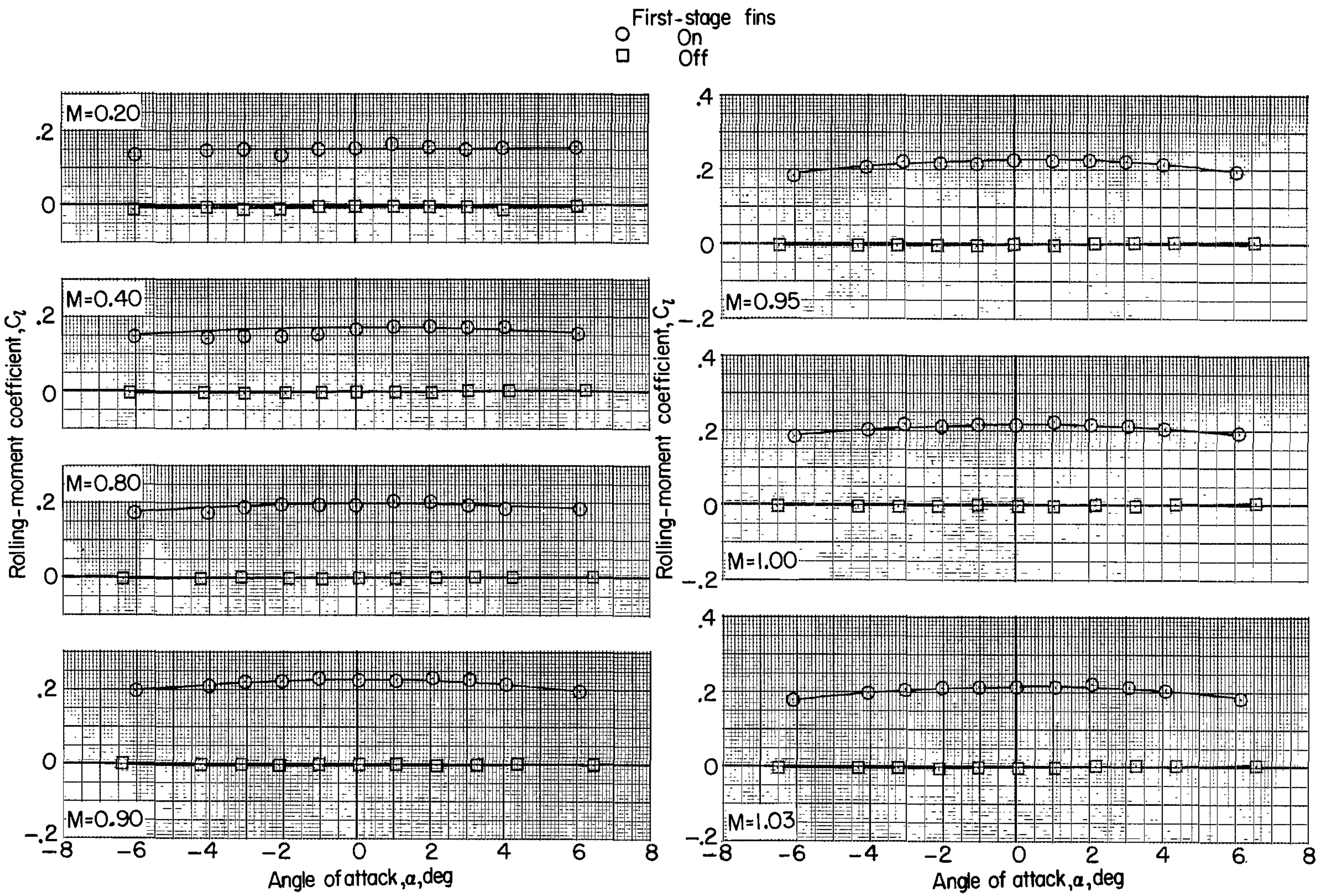

Figure 9.- Variation of rolling-moment coefficient with angle of attack.

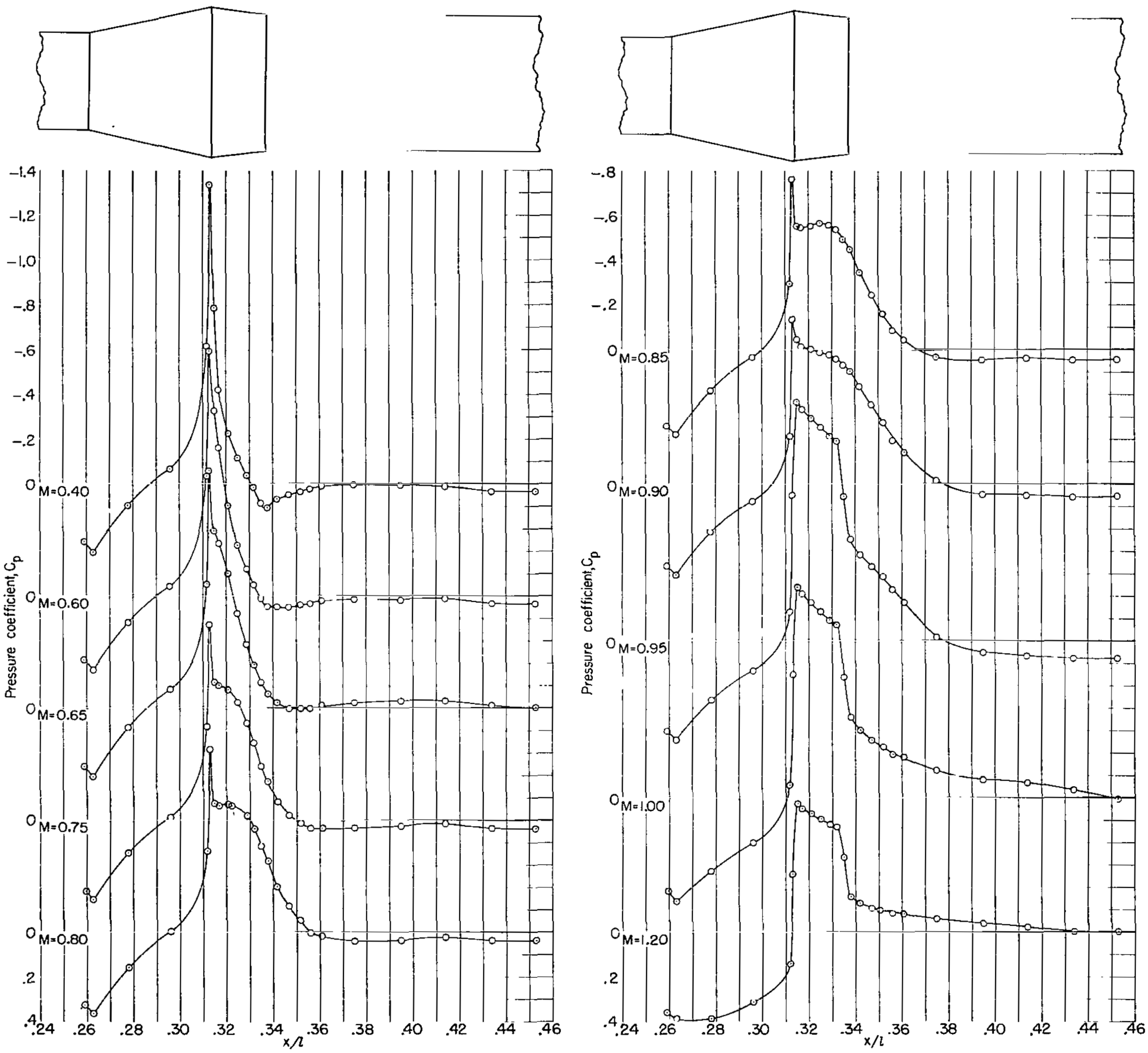

Figure 10.- Surface pressure distribution for flare—reverse-flare transition section. $\alpha = 0^{\circ}$; $\phi = 0^{\circ}$.

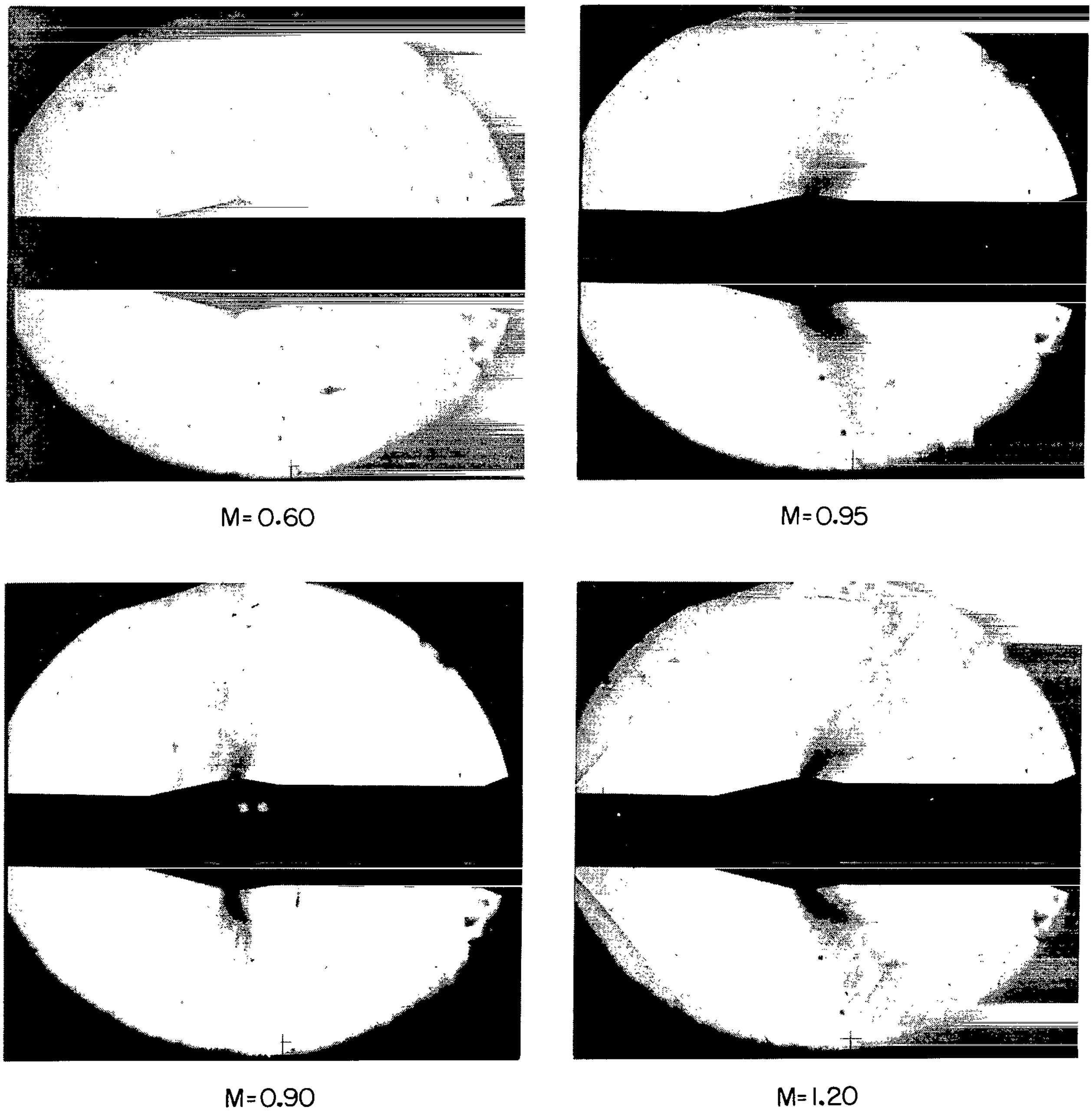

Figure 11.- Schlieren photographs. Flare—reverse-flare transition section; $\alpha = 0^{\circ}$. L-64-358

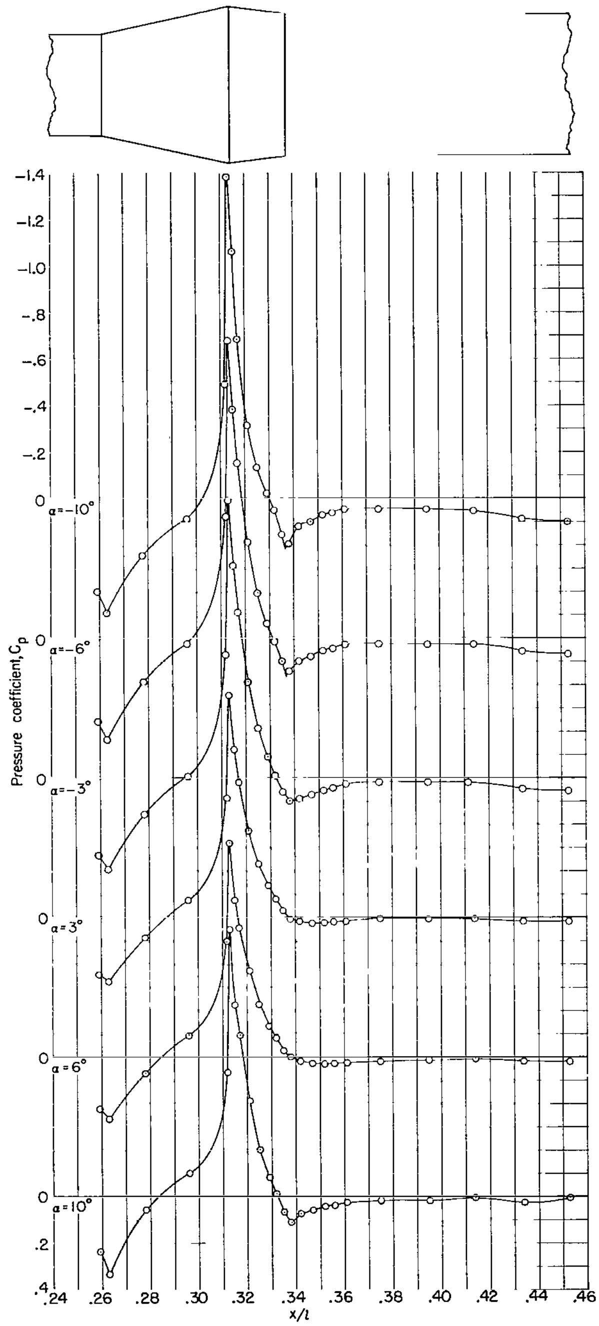

(a) M = 0.60.

Figure 12.- Effect of angle of attack on surface pressure distributions for flare—reverse-flare transition section. $\phi = 0^{\circ}$.

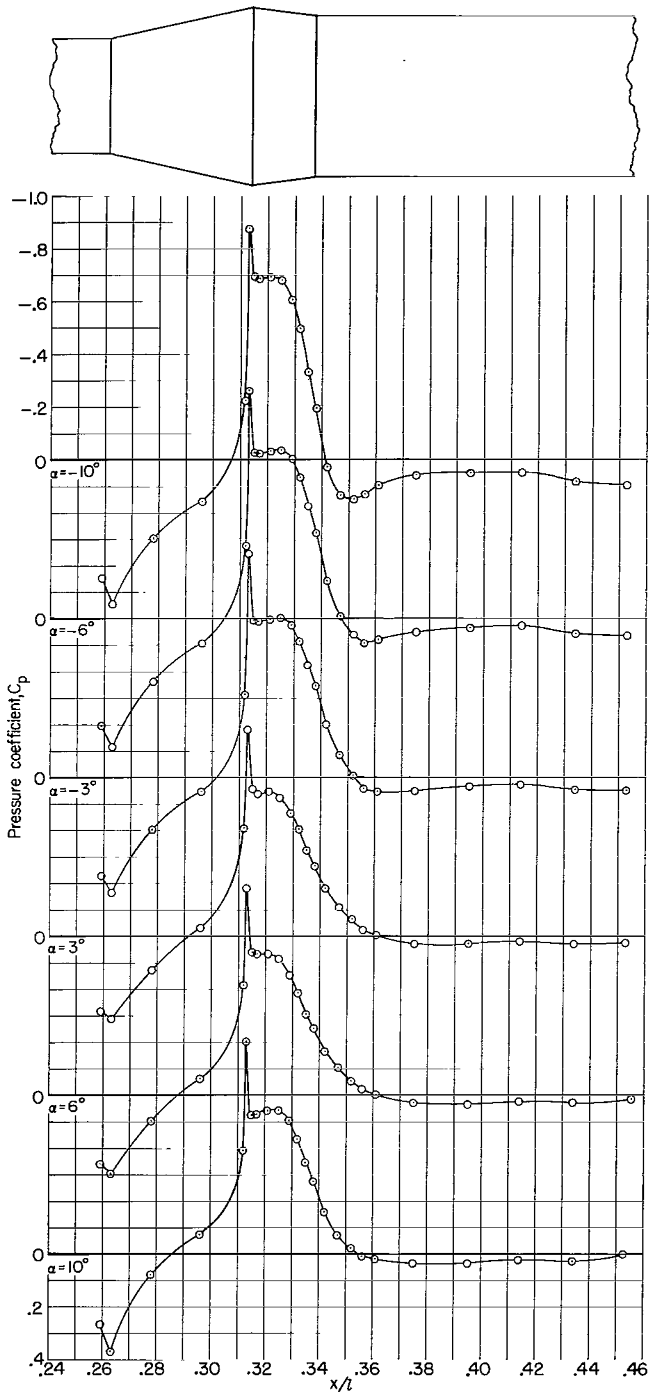

(b) M = 0.80.

Figure 12.- Continued.

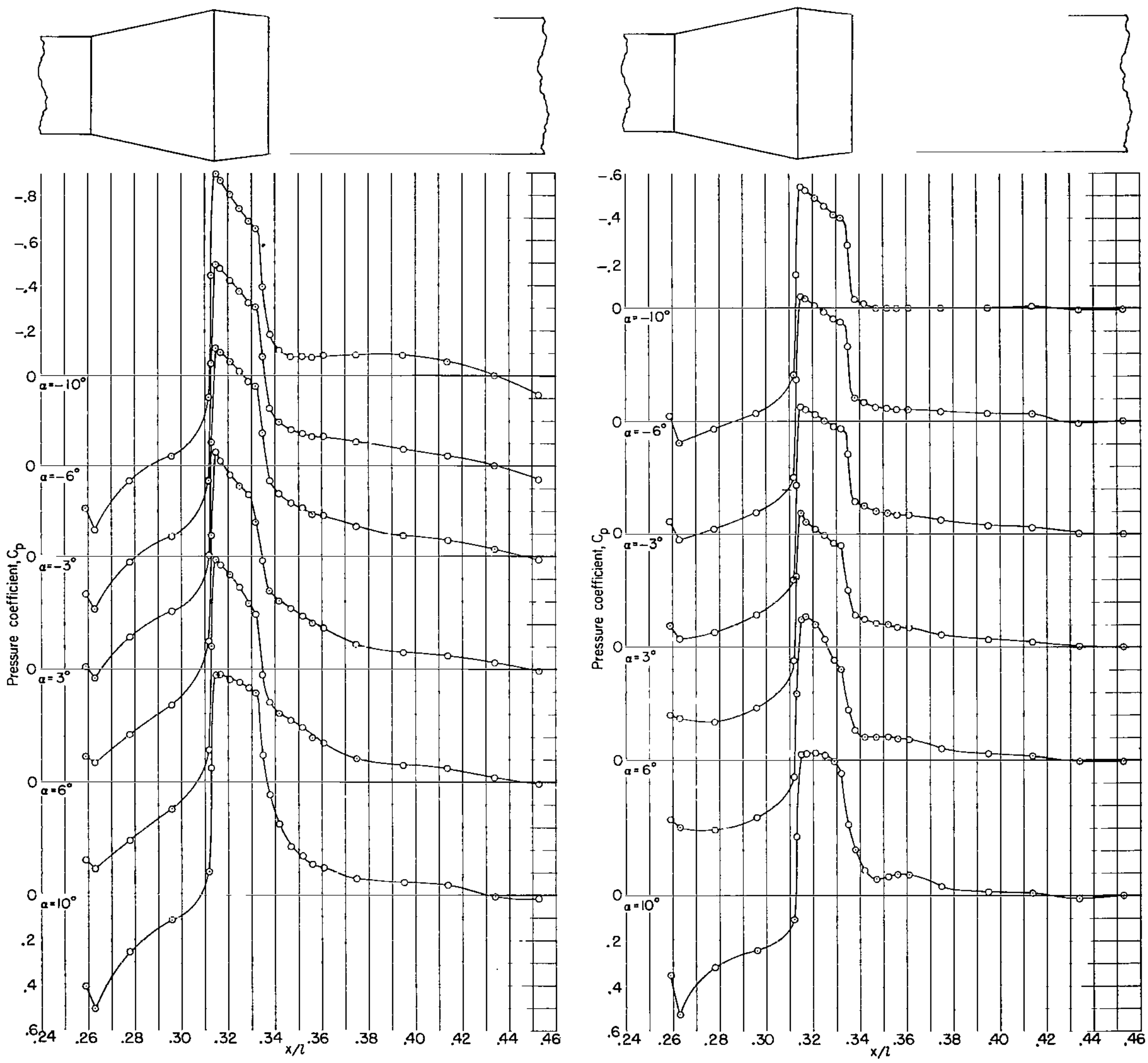

(c) M = 1.00. (d) M = 1.20.

Figure 12.- Concluded.

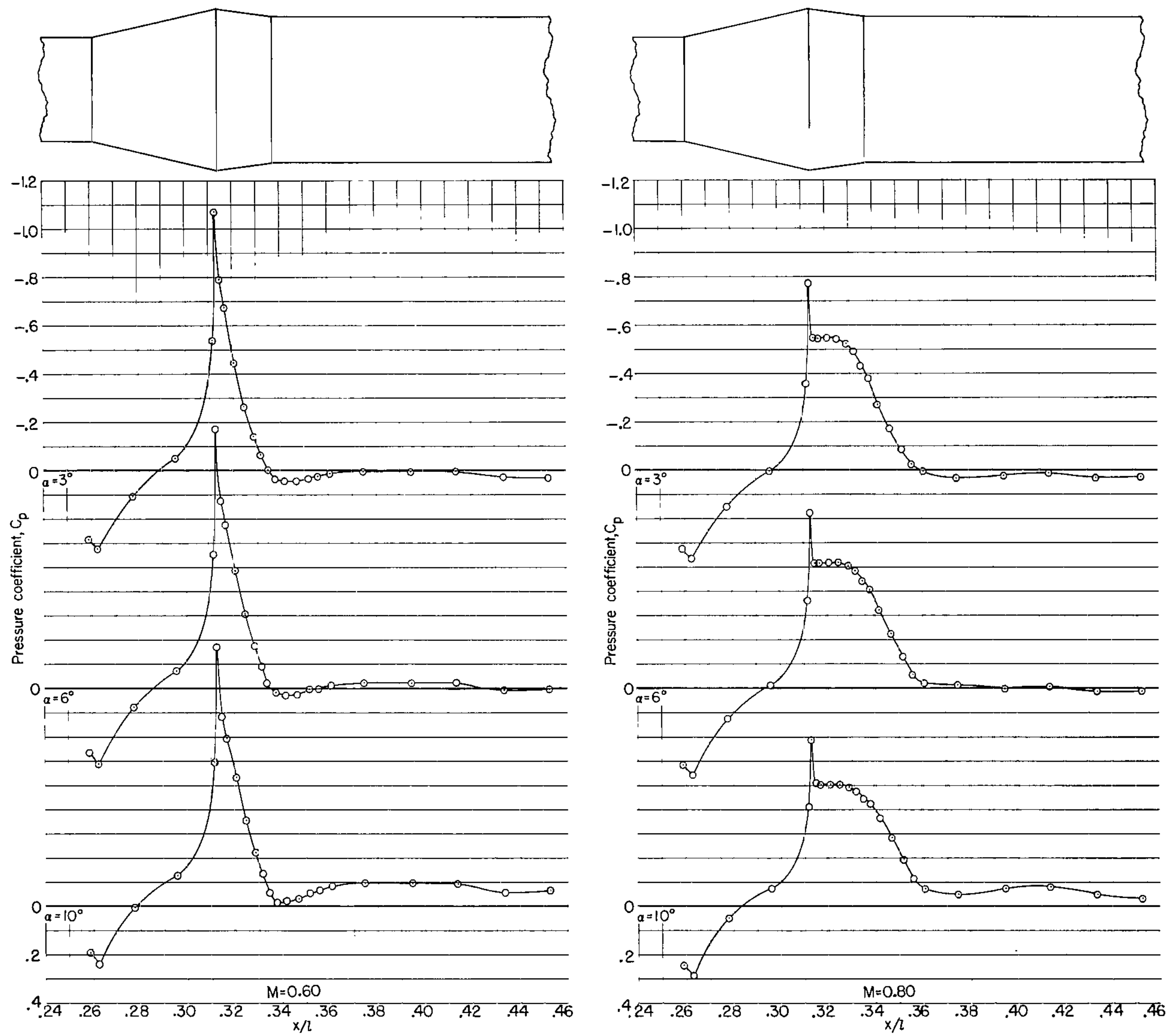

(a) M = 0.60 and M = 0.80.

Figure 13.- Effect of angle of attack on surface pressure distributions for flare—reverse-flare transition section. $\phi = 90^{\circ}$.

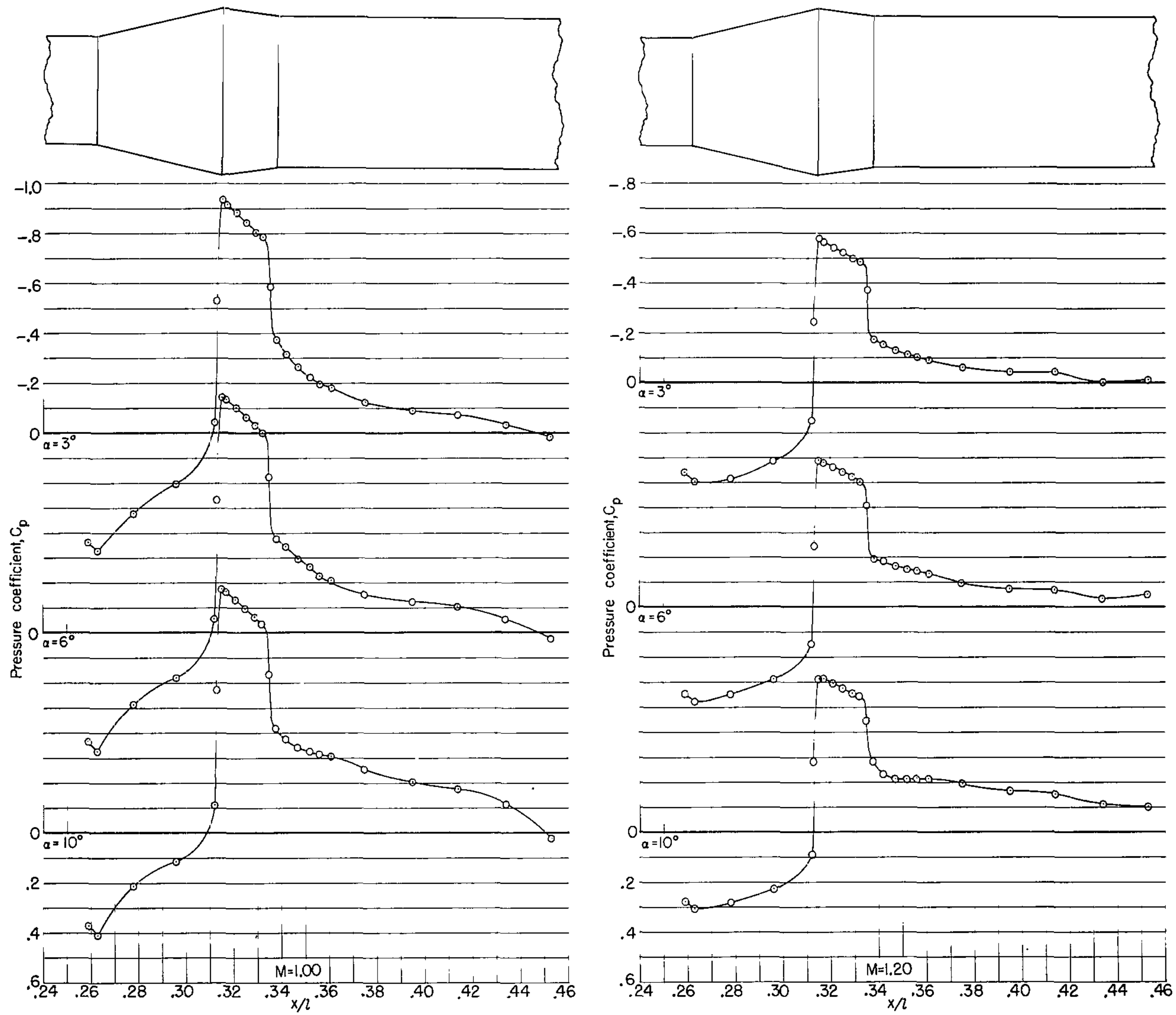

(b) M = 1.00 and M = 1.20.

Figure 13.- Concluded.

NASA-Langley, 1964 L-3673

"The National Aeronautics and Space Administration . . . shall . . . provide for the widest practical appropriate dissemination of information concerning its activities and the results thereof . . . objectives being the expansion of human knowledge of phenomena in the atmosphere and space."

—National Aeronautics and Space Act of 1958

NASA SCIENTIFIC AND TECHNICAL PUBLICATIONS

TECHNICAL REPORTS: Scientific and technical information considered important, complete, and a lasting contribution to existing knowledge.

TECHNICAL NOTES: Information less broad in scope but nevertheless of importance as a contribution to existing knowledge.

TECHNICAL MEMORANDUMS: Information receiving limited distribution because of preliminary data, security classification, or other reasons.

CONTRACTOR REPORTS: Technical information generated in connection with a NASA contract or grant and released under NASA auspices.

TECHNICAL TRANSLATIONS: Information published in a foreign language considered to merit NASA distribution in English.

TECHNICAL REPRINTS: Information derived from NASA activities and initially published in the form of journal articles or meeting papers.

SPECIAL PUBLICATIONS: Information derived from or of value to NASA activities but not necessarily reporting the results of individual NASA-programmed scientific efforts. Publications include conference proceedings, monographs, data compilations, handbooks, sourcebooks, and special bibliographies.

Details on the availability of these publications may be obtained from:

SCIENTIFIC AND TECHNICAL INFORMATION DIVISION

NATIONAL AERONAUTICS AND SPACE ADMINISTRATION

Washington, D.C. 20546